Transparent photovoltaic technologies: Current trends towards upscaling

Transparent photovoltaic technologies: current trends towards upscaling

Emilio **Pulli**,[1] Elena **Rozzi**[1] and Federico **Bella**[2,*]

1) Department of Energy, Corso Duca degli Abruzzi 24, 10129 – Torino, Italy
2) Department of Applied Science and Technology, Politecnico di Torino, Corso Duca degli Abruzzi 24, 10129 – Torino, Italy

Corresponding author: Federico Bella (federico.bella@polito.it, +39 0110904643).

Abstract. The world energy scenario is now living significant contributions coming from the photovoltaic field: new organic/inorganic hybrid materials have emerged in recent years, and in some cases these emerging strategies have exceeded the performance of traditional crystalline silicon. The next step concerns the integration of these technologies in smart buildings, in order to maximize the active surface capable of producing electricity and to contain the costs of air conditioning without affecting the amount of light needed. This review focuses on some of the most recent strategies developed to this purpose. Following an initial background on solar cells and figures of merit to characterize a transparent photovoltaic panel, the manuscript deals with a thorough analysis of wavelength-selective and non-wavelength selective devices, mentioning the main outcomes in the recent years. This distinction is proposed for both solar cells and solar concentrators, two areas in rapid evolution in academia and company worlds. A newly proposed case study and the example of a pre-industrial reality that has just started to scale-up this technology conclude this review, leaving to the reader a rich background on this highly-in-vogue field.

Keywords: Solar energy; Transparent photovoltaics; Energy consumption; Building-integrated photovoltaics; Financial analysis; Transparent solar cell.

List of abbreviations:

AgNWs = silver nanowires
AVT = average visible light transmittance
BIPV = building-integrated photovoltaic
CIGS = copper indium gallium diselenide
COP = coefficient of performance

DSSC = dye-sensitized solar cell

EER = energy efficiency ratio

EPD = electrophoretic deposition

ETL = electrons transporting layer

FTO = fluorine-doped tin oxide

HTL = holes transporting layer

ITO = indium-doped tin oxide

LSC = luminescent solar concentrator

MPPT = maximum power point tracking system

NIR = near-infrared

NPV = net present value

OPV = organic photovoltaic

PBDTT-DPP = poly(2,6′-4,8-bis(5-ethylhexylthienyl)benzo[1,2-*b*;3,4-*b*]dithiophene-*alt*-5-dibutyloctyl-3,6-bis(5-bromothiophen-2-yl)pyrrolo[3,4-*c*]pyrrole-1,4-dione)

PBT = payback time

PCBM = [6,6]-phenyl-C_{61}-butyric acid methyl ester

PCE = power conversion efficiency

PEDOT:PSS = poly(3,4-ethylenedioxythiophene):poly(styrenesulfonic acid)

PIPV = product-integrated photovoltaic

polyTPD = poly(N,N'-bis-4-butylphenyl-N,N'-bisphenyl)benzidine

PSC = polymer solar cell

PV = photovoltaic

PVGIS = Photovoltaic Geographical Information System

PVSC = perovskite solar cell

QD = quantum dot

SSC = scattering solar concentrator

TCO = transparent conducting oxide

TFPV = thin film photovoltaic

TLSC = transparent luminescent solar concentrator

TPV = transparent photovoltaic

TSC = transparent solar cell

UV = ultraviolet

1. Introduction

The demand for novel sustainable energy sources has become one of the most challenging topics addressed by worldwide researches in the last years [1,2], which stems from the increasing development of a consumerist world. Industrialization and rapid growth of global population have catalysed a search for practical renewable energy sources with the huge aim of fossil fuels replacement [3,4]. However, pushing global energy consumption far from fossil fuels demands for novel and not expensive technologies for the conversion of sustainable sources [5,6].

Due to its accessibility, cleanliness and abundance, solar energy has emerged as the most promising choice for the plan of a concretely sustainable world [7,8,9]; it is utilised in different ways, such as for heating water, producing electricity through photovoltaic (PV) technologies, etc. [10,11,12,13,14]. PVs can fulfil this demand many times over if adopted over a wide scale [15,16,17,18,19]. As an example, a PV installation covering around 20% of a region like Nevada can provide energy to the whole United States [20]. However, currently the installed PV plants only satisfy around 1% of the global energy demand [20]. Moreover, a really important barrier to the further growth of a solar energy scenario and the large-scale installation of PV technologies is given by the relatively weak energy density of sun irradiation in comparison to the energy demand [21,22]. Given that such a small portion of the global energy requirement can be satisfied by the nowadays installed PV plants, mainly in isolated and particularly sunny regions, it is required to boost the solar energy-related infrastructure if the real aim of the society is that of convert enough light to compensate for a relevant amount of non-renewable energy consumption.

This issue drove researchers to design new PV concepts, like transparent solar cells (TSCs), that can solve the problem by turning any sheet of glass (or, in general, a transparent substrate) into a PV device. The resulting solar cells are able to provide power by capturing and making use of light through windows in buildings and vehicles, leading to a truly efficient use of architectural spaces, also ensuring definitively better aesthetic features. Several transparent PV (TPV) technologies are investigated in this review as the most representative of the state of art; their main aim is that of achieving important transparency together with an electrical response compatible with that of PV modules currently sold in the global market. Furthermore, keeping in mind the extreme potential applications of TPV technologies in modern buildings, semi-TSCs are also mentioned as a relevant example, since they contribute to the often-mentioned building-integrated PVs (BIPVs) [23,24,25]. In this framework, with the aim of analyzing these promising technologies also from a financial point of view, a case study based on a generic building with offices in Europe is proposed as a precious and concrete example. The present findings show that

these integrated systems would be able to generate electricity and also lower lighting and cooling energy demand. As a further success story, the case of an Italian start-up which has invested 2.25 M€ in TPV technology for BIPV application is reported as a clear signal of the high potential of this market.

2. Background

In the case the reader is not an expert in PV technologies, this section briefly summarizes the principle behind the PV effect. Furthermore, the main classes of PV cells are described, with particular attention to the emerging strategies based on hybrid, abundant and low-impact materials.

2.1. The structure and working principle of a photovoltaic cell

TPV technologies have recently caught the attention of scientists given their unique feature of transforming common products, such as windows and electronic devices, into power generators without altering how they normally appear or work. However, in order to properly examine the TPV technology, the operational principle of the most used PV cells needs to be described [26,27,28,29,30], together with a short background on the evolution that this technology experienced over the years leading to different kinds of solar cells.

A PV cell is a device able to convert solar light into electricity by means of semiconductors, e.g. crystalline solids, the properties of which are achieved under normal conditions by the use of dopants and impurities [31,32,33,34,35]. The semiconductor present in a PV cell captures sunlight (photons), and this allows electrons to form electrons and holes couples, that are then guided in one direction, thus allowing current generation. The semiconductor is doped to behave as a p-n junction bearing a voltage difference, that will drive current flowing through the device in one direction, so that it can be harvested as electricity. This phenomenon of electrons flow as a consequence of photons absorption represents the PV effect and is clearly shown in **Figure 1**. The diffusion length is among the main factors affecting the power conversion efficiency (PCE) of the PV device [36,37,38,39,40].

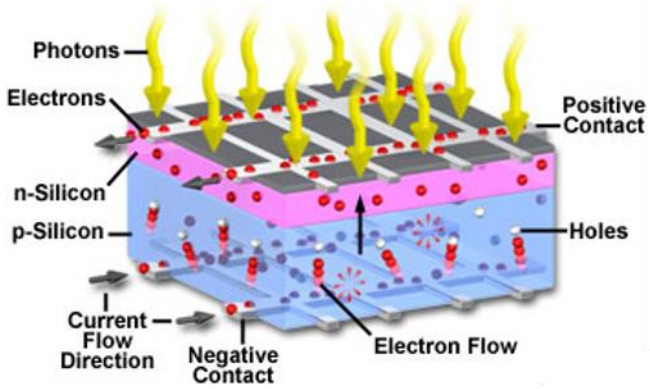

Figure 1. Schematic representation of a solar cell. Adapted and reprinted from [41].

2.2. The technological evolution of photovoltaic cells

The challenges that PV cells face concern cost, PCE and operating lifetime [42,43,44]. The scientific community is now focusing on developing suitable materials and fabrication processes that will improve the exploitation of the PV technology [45,46,47,48,49]. Silicon had been the first semiconductor that showed good PCE, obeying to the structure and operational principle described in Section 2.1 [31]. It is used for the fabrication of monocrystalline PV devices, that are at least 6% more performant, but also costlier than polycrystalline PV counterparts. Monocrystalline Si solar cells shows to be more electrically efficient, since they possess a defects-free crystal structure, while polycrystalline devices, based on multiple small silicon crystals, show lower performance, but are slightly cheaper to be produced [50,51]. Researchers have also proposed alternative materials and processing technologies that can lead to a similar PCE, and this led to the second generation of PVs, mainly populated by thin film PV (TFPV) cells [31]. Thin films possess the feature of reducing the quantity of semiconductor used for the preparation of PV cells, also reducing – in several cases – the cost by more than one half. Last, but not least, third generation solar cells emerged when hybrid and highly abundant materials were chosen as principal components of PV cells [52,53,54]; among the most known technologies, dye-sensitized solar cells (DSSCs) [55,56,57,58,59] and perovskite solar cells (PVSCs) [60,61,62,63,64] must be mentioned. A little background on DSSCs is given in the following section, since these cells, together with the standard silicon-based ones, are representing the main technology used to build PV modules/panels in both conventional and unconventional fields [65,66,67,68,69]. The current energy scenario is also pushing the PV community to try the integration of solar cells with batteries and supercapacitors, in order to concretely achieve smart cities and companies [70,71,72,73,74,75,76,77,78,79,80].

2.2.1. The structure and working principle of a dye-sensitized solar cell

Since the scientists O'Regan and Grätzel reported the fabrication of the first DSSC in 1991 [81], with PCE of 7-8%, this regenerative photoelectrochemical device became a promising solar energy converter [82,83,84,85]. DSSC is truly easy to being assembled, at low cost, and shows a high PCE [86,87,88,89,90], exceeding 14% at lab-scale level. These properties rapidly attracted scientists' and researcher's attention [91,92,93,94,95]. A well-designed DSSC possesses a combination of a dye-sensitized semiconductor anode (such as TiO_2, ZnO, SnO_2, Nb_2O_5), an electrolyte and a counter electrode [96,97,98,99,100]. The components of a DSSC are illustrated in **Figure 2**.

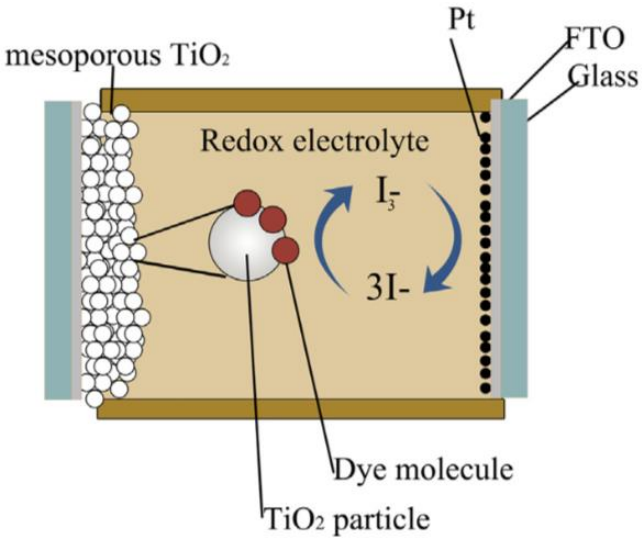

Figure 2. Schematic representation of a DSSC. Adapted and reprinted with permission from [31].

The core of a DSSC is the mesoporous semiconductor layer based on TiO_2 nanoparticles as a path for the electrons to cross from the excited dye molecules to the current collector [101,102,103]; the diameter of the nanoparticles ranges between 10 and 30 nm, while the layer thickness is around 10 μm [104,105,106,107,108]. The semiconductor layer is deposited on a substrate previously coated with a transparent conducting oxide (TCO) [109,110,111,112,113], such as the fluorine-doped tin oxide (FTO) [114,115,116,117,118]. After being excited by sunlight, the dye molecules inject electrons in the conduction band of the semiconductor and are then regenerated by electron donation from the redox shuttle present in the electrolyte [119,120,121,122,123]. The electrolyte in these solar cells contains the I^-/I_3^- species dissolved in an organic solvent, but quasi-solid and solid counterparts were also proposed [124,125,126,127,128]. The process of redox shuttle oxidation leads to the production of an excess of I_3^- ions, which are then regenerated by the electrons coming from the cathode, that is commonly

made of a thin layer of platinum [129,130,131,132,133]. Other compounds like carbon-based nanostructures and conducting polymers have been widely studied to replace Pt given its important cost, weak corrosion-resistance and scarce abundance [134,135,136,137,138].

Of note, integration of DSSCs into portable products is leading to a new field called product-integrated PV (PIPV) [139,140,141,142,143]. This further pushed the research community towards the development of suitable cell components [144,145,146,147,148].

3. Review of main transparent photovoltaics technologies

The core of this review is the analysis of the state of the art of TPVs and its use for many applications, particularly regarding windows in buildings. Transparency is the physical property of allowing the transmission of light through a material. What makes a material transparent is the intrinsic arrangement of its atoms and electrons. When the incident photons have a sufficient energy to make the electrons of the semiconducting material move to a higher energy state level, light passes through that material, making it opaque (**Figure 3A**). The principal feature of a solar cell is that of absorbing light, and now the scientific community is trying to boost the transparency of PV devices without reducing too much their efficiency.

Considering this ambitious goal, the development of TPVs is carried out keeping in mind these two factors:

- *Average visible light transmittance (AVT)*, which is determined by selecting the average of device transparency in the visible portion of the spectrum (400-700 nm) based on the spectrally-dependent response of the human eye [149].
- *PCE*, which is intended as the ratio of energy output from the PV device with respect to the energy input from the sun. Besides reflecting the efficiency of the PV device itself, the PCE is function of the spectrum and intensity of the incident solar light and the temperature of the solar cell. As a consequence, the conditions under which PCE is determined have to be carefully checked with the aim of precisely comparing the efficiency of a cell to another [150].

The main aim of realizing a technology able to have a high AVT without affecting its PCE led to two main categories of TPVs [20]:

- *Wavelength-selective technologies*, which make use of photoactive compounds that preferentially harvest ultraviolet (UV) and near-infrared (NIR) radiation, while selectively transmitting the visible wavelengths (**Figure 3E-F**). These devices have already shown AVT values of 50-90%.

- *Non-wavelength-selective technologies*, which generate electricity from a wide absorption of sunlight (of course, visible portion included) and reach AVT through segmenting opaque devices (**Figure 3B**) or making use of a really thin or small amount of photoactive material (**Figure 3C-D**). They show AVT values included between 0 and 50% and are relevant for uses in colored windows and decorative outdoor architectures.

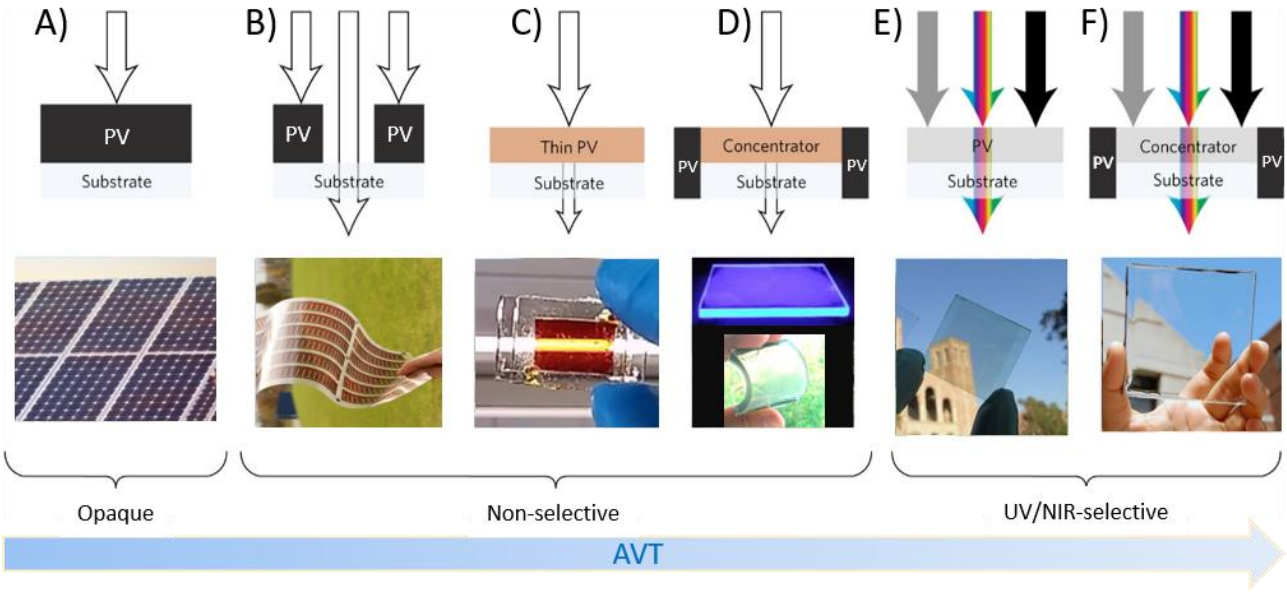

Figure 3. Trend of AVT property according to different classes of PV technologies, with a diagram and a digital picture of each example. **A)** A traditional opaque PV device where full spectrum sunlight (indicated by white arrows) is not transmitted. **B)** Spatially segmented PV device, where opaque modules on a transparent substrate are spaced to partially allow transmission of all wavelengths: increasing the distance among modules boosts transmission sacrificing performance, since this lowers the active area of the combined module. **C)** A non-wavelength-selective TFPV device, where the thickness of the absorbing film(s) is modulated to equilibrate AVT and PCE, since raising the thickness improves PCE at the cost of partial transmission (narrow white arrows) and color rendering. **D)** Diagram of a non-wavelength-selective solar concentrator, colored luminescent solar concentrator (LSC) and a scattering solar concentrator (SSC): light is collected by harvesting, re-emitting, and waveguiding photons from a sensitizer or by scattering impimping photons toward the edges of a substrate, to be then collected by edge-mounted PV cells. **E)** A wavelength-selective TPV device. **F)** A wavelength-selective LSC; wavelength-selective TPV technologies preferentially absorb UV (grey arrows) and NIR (black arrows) light, while allowing the transmission of visible light (colored arrows). Scheme inspired from [20], but containing digital pictures updated in 2020 from authors' archive.

There are a few technologies that can be exploited to develop TPV products, and they represent a milestone of present research efforts due to the market demand and their potential uses. The research centers that publish and patent some success stories with TPV are mainly located in Japan, USA, Germany and India. The forthcoming sections detail the development and performance issues of TPV technologies, including TSCs, LSCs and SSCs; a particular focus will be given to

those technologies that demonstrated the ability to target a transmittance higher than 20% and with a PCE higher than 1%, by highlighting their structures and fabrication processes.

3.1. Transparent solar cells technologies

Research efforts on TSCs largely focused on strategies to segment opaque solar cells, lowering the thickness of otherwise opaque photoactive thin films, or on exploiting UV/NIR wavelength-selective photoactive compounds to reach visible light transmission. In these paragraphs, different approaches to TSC technologies are examined according to the two main categories of wavelength and non-wavelength selective technologies mentioned above. However, the materials that will be mentioned are not strictly related to a single type of TPV concept; conversely, a material used for a wavelength-selective solar cell can often be applied for a non-wavelength-selective device according to a different fabrication method. Consequently, the analysis of the technologies described below should be done by taking into account the whole fabrication process and cell geometry, without simply focusing on the single photoactive material.

It should also be emphasized that current research is very active with the challenging aim of using emerging concepts in the fields of nanomaterials [151,152,153,154,155,156,157], photocatalysis [158,159,160], design of sensitizers [161,162,163,164,165], electrochromics [166,167,168,169,170], semiconductors [171,172,173], polymers [174,175,176,177,178,179,180] and smart materials [181,182,183,184,185,186,187,188] for the preparation of new PV-compatible compounds [189,190,191,192,193,194,195,196].

3.1.1. Wavelength-selective thin film solar cells

Technologies transparent to human eye recently came to the attention of the scientific community by exploiting compounds that selectively absorb UV and/or NIR light (**Figure 3E**) [197,198]. These active materials are typically small organic molecules, nanotubes, polymers and salts [199,200,201]. From a chemical point of view, these kinds of solar cells base their principles on the fact that optical absorption in semiconductors (both organic and molecular ones) takes place in different molecular orbitals (S_1, S_2, ..., S_n) from the ground state (S_0). Consequently, the energy gap between S_1 and S_2 levels can be purposely used to permit the transmission of visible light and UV/NIR-selective absorption through a precise control of the molecular skeleton. By tailoring the band-gap and the discontinuity of states, research groups demonstrated the possibility to specifically tune the solar absorption outside the visible portion and into the NIR wavelengths.

In 2011, Lunt *et al.* followed the aforementioned criteria by designing dye molecules able to absorb UV and NIR (650-850 nm) wavelengths [202]. Their concept was based on a heterojunction organic PV (OPV) cell able to absorb sunlight in the NIR spectrum, showing an AVT of 65% and a PCE of 1.3 ± 0.1%. The cell contained chloro-aluminium phthalocyanine as a molecular organic donor and C_{60} as an acceptor. The cell anode was coated with indium-doped tin oxide (ITO), ClAlPc, C_{60}, bathocuproine and MoO_3, while the cathodic side contained a Ag layer deposited by thermal evaporation. The growth of the transparent NIR mirror was carried out separately onto a quartz substrate and constituted a distributed Bragg reflector. TiO_2 and SiO_2 films were sputtered to obtain a precise thickness useful to generate a stop band of around 88 nm. At the opposite part of the quartz, a broadband antireflection film was deposited. The overall scheme of the cell is shown in **Figure 4A**; the principal aim of the presented TSC geometry was to permit visible wavelengths to pass through and harvest UV and NIR portions. To demonstrate the operation of the TSC, its absorptive response was measured and then compared with that of a conventional solar cell (**Figure 4BC**), and the absorptive response (black curve) was superimposed on the solar spectrum (grey curve). In a conventional cell, the wavelengths at which absorption was relatively high included the visible part of the spectrum; conversely, the transparent cell absorbed well in the NIR and the UV portion of sunlight, but in the visible region the absorption dropped off, approaching zero.

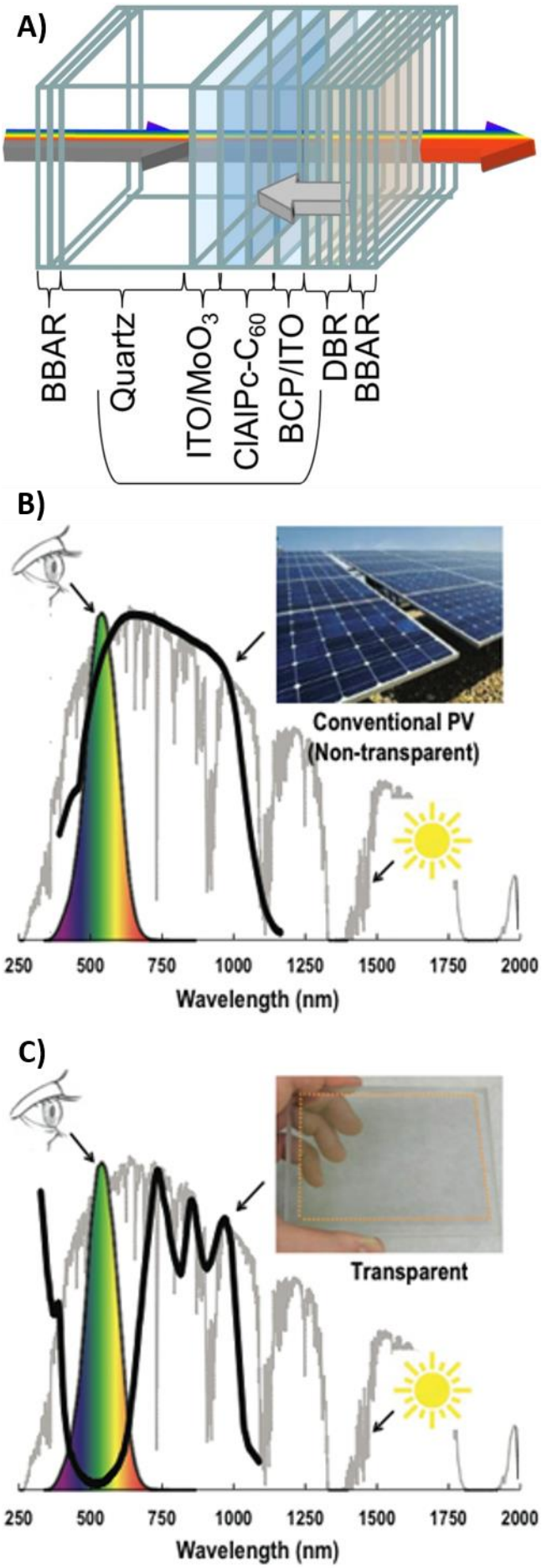
A)
BBAR
Quartz
ITO/MoO3
ClAlPc-C60
BCP/ITO
DBR
BBAR
B)
Conventional PV
(Non-transparent)
250
500
750
1000
1250
1500
1750
2000
Wavelength (nm)
C)
Transparent
250
500
750
1000
1250
1500
1750
2000
Wavelength (nm)

Figure 4. A) Scheme of a TSC. **B)** Spectral response of a conventional Si-based solar cell and of **C)** a TSC. Adapted and reprinted with permission from [202,203].

In 2012, Chen *et al.* checked the opportunity to produce TSCs by means of a solution processing technique [204]. With the golf of achieving an ideal TPV cell, the harvesting compound must absorb all the radiation in both UV and NIR portions and let visible light pass through the device (see **Figure 5A**). Some materials with these properties exist, like graphene and carbon nanotubes, that are both transparent and characterized by a proper conductivity; however, it is not efficient to simply adopt these compounds to fabricate a TPV device. Therefore, the suggestion coming from these authors was that of combining a transparent polymer solar cell (PSC) with a transparent conducting compound, like silver nanowires (AgNWs), thus creating a transparent PSC able to harvest both UV and NIR portions (sometimes these kinds of solar cells are referred as "semitransparent"). This photoactive layer consisted of a bulk heterojunction mixture based on the NIR wavelengths-sensitive polymer poly(2,6′-4,8-bis(5-ethylhexylthienyl)benzo[1,2-*b*;3,4-*b*]dithiophene-*alt*-5-dibutyloctyl-3,6-bis(5-bromothiophen-2-yl)pyrrolo[3,4-*c*]pyrrole-1,4-dione) (PBDTT-DPP, bearing strong absorption between 650 and 850 nm) as the electron donor and [6,6]-phenyl-C_{61}-butyric acid methyl ester (PCBM, working below 400 nm) as electron acceptor. The PBDTT-DPP:PCBM photosensitive substrate showed a maximum AVT of 73% at ≈550 nm, with a 68% values over the whole visible spectrum (400-650 nm), remaining successfully active also in the NIR portion (650-850 nm), as shown in **Figure 5B**. As regards the highly efficient transparent top cathode to be placed on the top of the photosensitive layer, a spray-coated AgNWs-laden composite was processed using alcoholic solvents compatible with standard PSC compunds.

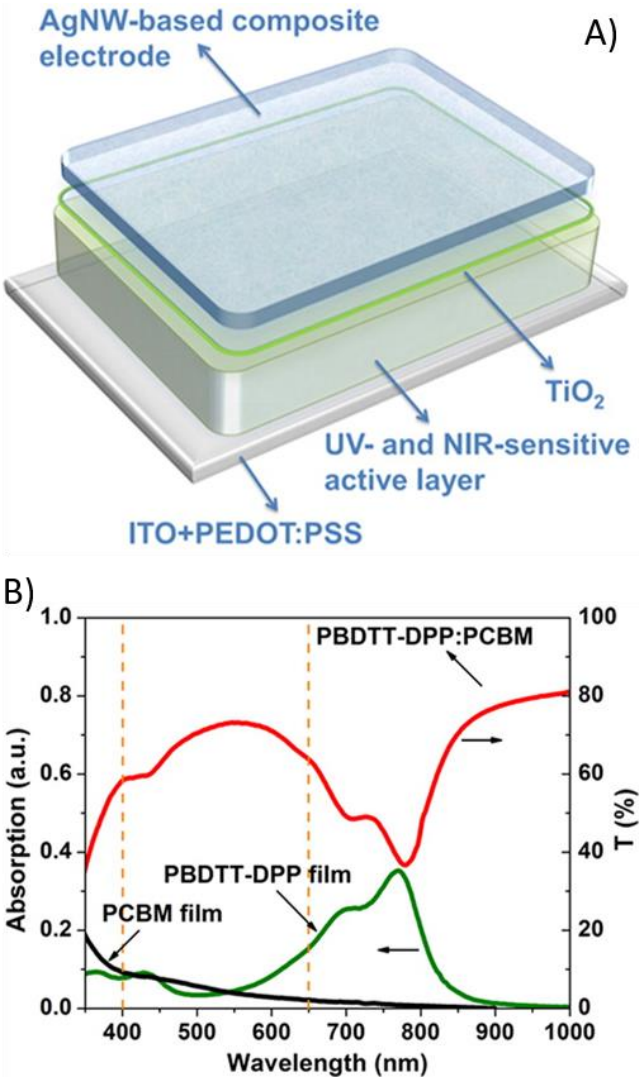

Figure 5. A) Schematic representation of a transparent solution-processed PSC. **B)** Absorption spectra of PBDTT-DPP and PCBM and transmission spectrum of the PBDTT-DPP:PCBM bulk heterojunction photosensitive layer; the dashed lines highlight the visible portion of the spectrum. Adapted and reprinted with permission from [204].

Another TSC technology that has recently gathered attention due to the impressive optoelectronic properties is based on quantum dots (QDs) [205]. In this field, transparent and semi-transparent QDs-sensitized solar cells are emerging as leading technologies. Zhang *et al*. published two TSCs concepts based on QDs [206]. The first approach was based on PbS QDs with a tuneable band-gap, leading to an excellent light absorber for PV cell applications and achieving 9% PCE. Additionally, these QDs were transparent and showed an intriguing feature of multi-exciton generation, where a photon produced more than one electron-hole pair. The PbS QDs-based solar cell was fabricated onto a FTO glass, matching a TiO_2 film as an electrons transporting layer (ETL) and a MoO_3 film as holes transporting layer (HTL); moreover, the difunctional ligand 3-mercaptopropionic acid was added to boost the charge carriers mobility within the QDs film.

Through modifying the thickness of the QDs layer, the PCE varied passing from 2.04% to 3.88%, and the AVT ranged from 32.1% to 22.7%. The second device proposed by Zhang *et al.* achieved a 5.4% PCE and an AVT equal to 24.1%. The materials and the architecture chosen to fabricate this cell helped to lower optical losses, which eventually increased the PCE, making it adapt for uses characterized by low transmittance requirements.

3.1.2. Non-wavelength-selective solar cells, spatially segmented photovoltaics

Spatial segmentation is the process based on the dispersion of opaque PV devices across transparent substrates. This strategy leads to various levels of neutral optical transmission through the space present between difference PV cells. Increasing these areas leads to the improvement of transmission and worsening of performance, since this approach lowers the photosensitive area [20].

Due to the fact that the scientific community focuses on the improvement of the semi-transparent nature of hybrid PV devices by utilizing a harvesting material bearing a band-gap lower than photons, the resulting strategy will permit visible radiation to pass through smart windows while absorbing NIR photons. However, the improvement of transparency makes PCE inevitably affected. As a consequence, big efforts towards the research of a potentially transparent material that improves cell PCE are spent, e.g. methyl ammonium lead halide in the form of perovskite [207,208,209,210,211]. Most of the highly efficient PVSCs are typically fabricated sandwiching a metal oxide material, the perovskite, and charge transporting materials [212,213,214,215,216]. Synthesized perovskites are hybrid materials that show good electric and optical properties [217,218,219,220,221,222], valid for PV devices application, like high carriers mobility and absorption coefficient, direct band-gap and suitable structural stability [223,224,225,226,227]. Most PV devices fabricated with perovskite crystals demonstrate the ability of targeting a PCE higher than 25% [228].

A semi-transparent perovskite was demonstrated by Roldán-Carmona *et al.*, with 6.4% PCE and 29% AVT, by choosing a perovskite evaporation deposition, that is a robust strategy enabling the progressive deposition of layers at low thickness (lower than 40 nm) [229]. This approach used an ultra-thin gold electrode (6 nm) capped with a LiF film with the aim of reducing energy losses. The thickness reduction caused a transmittance increase. Further, the LiF layer modified the circulation of the electric field within the device. The device was composed of several layers (see **Figure 6AB**), namely poly(3,4-ethylenedioxythiophene):poly(styrenesulfonic acid) (PEDOT:PSS), poly(N,N'-bis-4-butylphenyl-N,N'-bisphenyl)benzidine (polyTPD), $CH_3NH_3PbI_3$, $PCBM_{60}$, Au and LiF. One year later, Bailie *et al.* published a tandem PV device where a

transparent AgNWs electrode was deposited on the top of PVSCs to achieve semi-transparent devices. These latter were placed into a mechanically-stacked tandem architecture onto copper indium gallium diselenide (CIGS) and low-quality multicrystalline silicon [230]. The 12.7% efficient semi-transparent PVSC combined with the 17.0% efficient CIGS cell led to a 18.6% PCE in the tandem device, the scheme of which is shown in **Figure 6C**.

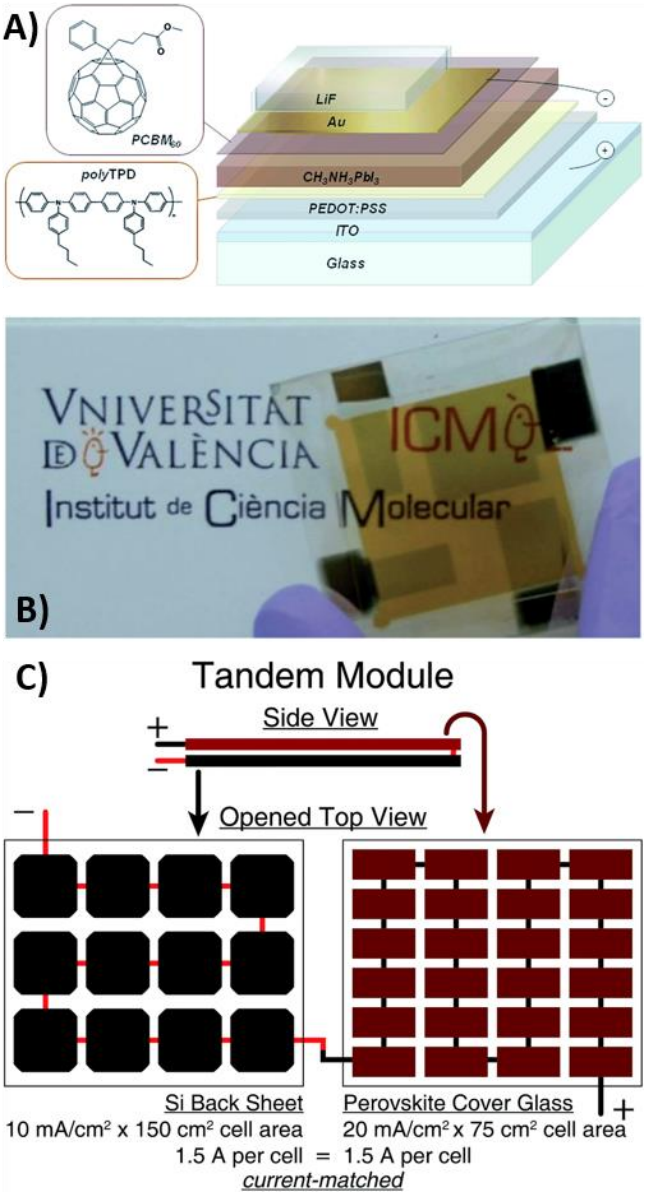

Figure 6. A) Scheme of a semitransparent PVSC (also showing the chemical structures of the organic holes and electrons blocking materials) and **B)** digital picture of the device. **C)** A perovskite/silicon (or CIGS) module with a simplified geometry and current density to show how current-matching at the module level can occur with a mechanically-stacked tandem. Here the filtered silicon produces half of the photocurrent density of the perovskite, so the silicon devices are twice as large to target the current of the perovskite unit. Adapted and reprinted with permission from [229,230].

3.1.3. Non-wavelength-selective solar cells, thin film photovoltaics

TFPV is among the most successful technologies for TSCs and comprehends several fabrication strategies. Part of these processes are function of materials and pastes preparation to achieve transparency requirements, while others approaches are based on the deposition of active materials onto FTO glasses. In this part of the review, the deposition strategies are highlighted and – for each of them – the preparation of pastes and active materials will be detailed.

TFPV is based on thin-film materials bearing thicknesses from a few nanometres up to tens of micrometres of photoactive compound deposited on glass by several approaches [31]. Indeed, it is rather simple to deposit thin layers on several substrates, both flexible and rigid, as well as insulators or metals. Through lowering the film thickness, transparency lowers. TFPV devices can be prepared by these frequently-mentioned technologies: screen-printing, electrophoretic deposition (EPD), dip-coating and sputtering.

Screen-printing is among the best method for the deposition of thin films and is largely applied in the PV field [231,232]; indeed, it provides a simple way to tailor the geometry and the thickness of the final film. The success of a screen printing process depends on the quality of the initial paste. In the case of DSSCs [233,234,235,236,237], TiO_2 nanoparticles are used for preparing the paste to fabricate photoanodes. The transparency is function of the screen printing technical features, e.g. made through a screen based on a mesh stretched over a frame; characteristics such as mesh opening and count, thread diameter, fabrication thickness and open surface are at the basis of the resulting film thickness and porosity. Moreover, the transparency can be controlled by the speed and pressure applied on the squeegee. **Figure 7A** highlights a typical screen printing process for TiO_2 paste deposition onto a conductive substrate.

EPD is an alternative strategy to obtain thin films and it is possibly to carry out this process in two steps [238,239]. The deposition of a thin film onto a FTO glass starts with particles spreading onto the glass by applying a direct voltage between two electrodes, thus creating an electric field. In this setup, one electrode behaves as a cathode, the other as an anode, and both of them are immersed into a solvent containing the particles. The second processing step is based on the gathering and deposition of synthesised particles onto one of the electrodes, with the resulting formation of a thin layer. The process is shown in **Figure 7B**.

A dip-coater (**Figure 7C**) is an instrument used to ensure high precision in the deposition process, the latter including five steps: i) Immersion: the substrate is placed into the solution of the coating compound; ii) Start-up: the substrate starts to be pulled up; iii) Deposition: the deposition of the thin layer on the substrate takes place, while it is pulled up at a constant speed;

iv) Drainage: the excess of liquid will drain from the surface; v) Evaporation: the solvent evaporates leaving the liquid phase, thus allowing to the obtainment of a thin layer [240,241].

Sputtering is another strategy to deposit thin films for PVs, based on a process where microscopic particles of a solid material are ejected from a target material when it is bombarded by energetic particles of a plasma or gas (see **Figure 7D**) [242,243]. A thin titanium nanotubes layer or a Pt counter electrode can indeed be deposited on FTO by sputtering.

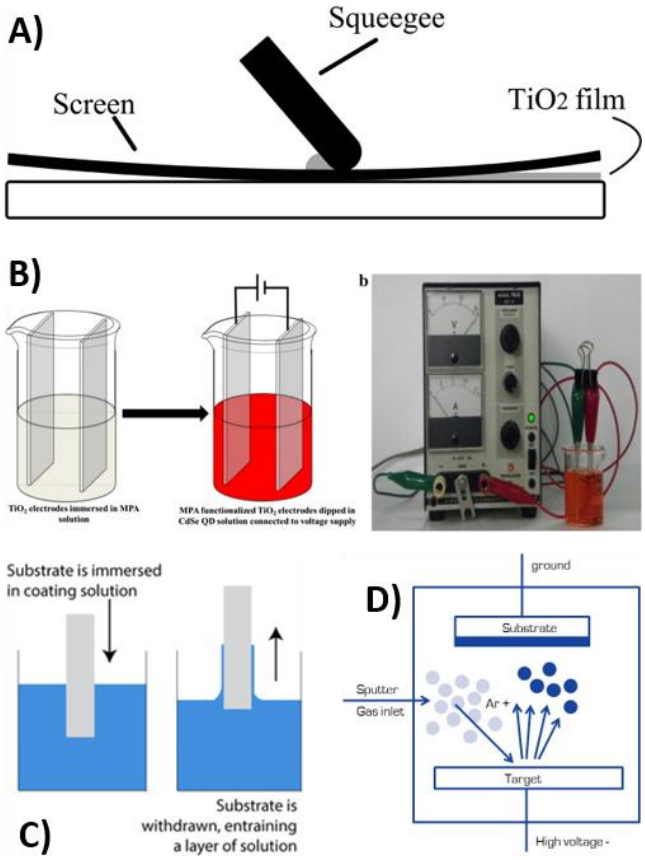

Figure 7. Schemes of processes for thin-film depositions: **A)** Screen-printing; B) EPD (with digital picture of the setup); C) Dip-coating; D) Sputtering. Adapted and reprinted with permission from [31,244,245,246].

3.2. Solar concentrator technologies

Solar concentrators are based on photoactive species or scattering effects to harvest the incident radiation normal to a substrate surface and redirect it at the edges, allowing it to be absorbed a by standard PV unit [247,248]. This paragraph describes the current work behind luminescent solar and scattering concentrators according to the same classification previously used for TSCs, based on wavelength and non-wavelength-selective technologies.

3.2.1. Non-wavelength-selective and colorful luminescent solar concentrators

A LSC is based on a substrate coated or embedded with an organic dye bearing the function of redirecting the incident radiation towards the edges by means of a photoluminescence phenomenon[249]. Its operating principle lies on the process here described: a part of sunlight is harvested by a luminescent species or luminophore incorporated into a transparent waveguide. The harvested sunlight is subsequently re-emitted at a different wavelength in an isotropical way, i.e. in all directions within the waveguide. Given the presence of a refraction index difference among the ambient environment and the waveguide, the re-emitted photons are quite all blocked by total internal reflection, leading to their redirection towards the waveguide edges. Here, they are converted to electrical power in a PV unit mounted at the edge. Overall, the system power efficiency, η_{LSC}, can be calculated by this equation:

$$\eta_{LSC} = \eta_{opt} \cdot \eta^*$$

where η_{opt} is the optical efficiency and represents the ratio between the number of photons transported out of the LSC edge and the impimping photons on the active area in spite of η^*, which represents the PCE of the edge-mounted PV unit under a monochromatic irradiation coming from the luminescent emitter [17]. Moreover, the optical efficiency is defined according to:

$$\eta_{opt} = \left(1 - R_f\right) \cdot \eta_{abs} \cdot \eta_{pl} \cdot \eta_{trap} \cdot \eta_{ra}$$

where R_f is the front-face reflection, η_{abs} is the absorption efficiency, η_{pl} is the luminescent efficiency, η_{trap} is the waveguiding efficiency, and η_{ra} is the efficiency of suppressing reabsorption.

The operating mechanism previously described is the same for non-wavelength and wavelength selective LSCs. The main difference between the two technologies is the different transmission of the visible region of the solar spectrum linked to the wavelength selective properties of the device. In fact, the non-wavelength-selective LSCs show colorful optical transmission because of the discrete visible harvesting.

3.2.2. Non-wavelength-selective scattering solar concentrators

SSCs are based on a uniform distribution of diffusive nanoparticles into a nanocomposite plate, the latter being sandwiched among two glass plates (**Figure 8**). When the impimping radiation from the sun passes through the first glass plate, the portion directed onto the nanocomposite is scattered in an irregular way by the embedded nanoparticles, being later transmitted in all the directions within the plate. Part of the radiation goes through the diffusive nanocomposite plate and penetrates the glass plate. The latter behaves as a second light-guiding substrate, due to its

refraction index differs from that of the diffusive nanocomposite plate. Part of the radiation is refracted at the moment it penetrates the diffusive nanocomposite plate, and the refracted photons later undergo a total internal reflection phenomenon occurring at the boundary of the glass plate. Some radiation at the end arrives at the silicon PV unit mounted at the device edges, where the sunlight is converted to electricity [250]. The intensity of the scattering and efficiency of the transmission strongly depend on the wavelength of the impimping radiation.

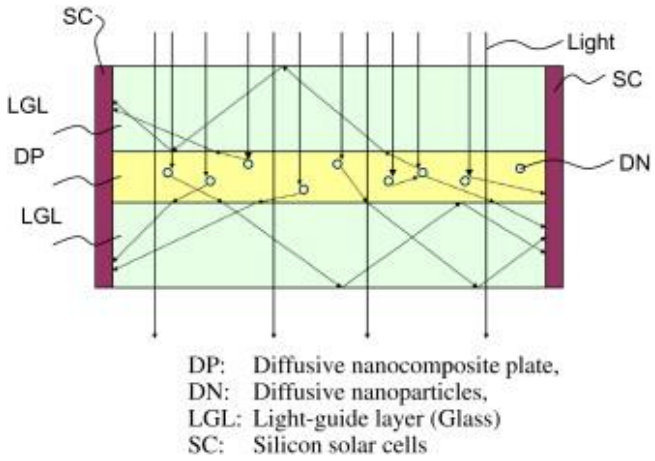

Figure 8. Scheme of light guided to PV devices through a radiation diffusive layer and light-guide layer. Adapted and reprinted with permission from [250].

Unfortunately, the principal challenge for a scattering concentrator is given by the significant optical losses, especially at area scales above a few inches. This is cause by the multiple scattering events of the waveguided photons, that can lead to important losses via outcoupling from the cell. As a consequence, this type of tecnology has registered PCE values of approximately 5% with AVT of 50-60%.

3.2.3. Wavelength-selective and transparent solar concentrators

The use of non-wavelength-selective LSCs is usually constrained by the absorption of the chromophore and relative emission in the visible wavelengths, that causes a wide degree of colored tinting. To overcome these hurdles, Zhao *et al.* reported another approach in 2014, called transparent LSC (TLSC) [251]. This technology harnesses the structured harvesting of sensitizing chromophores to fabricate LSC architectures able to selectively absorb NIR light by waveguiding deeper-NIR luminophore emission to highly performance segmented PV devices. TLSC can avoid the visual impact and lower the quantity of costly photovoltaic materials necessary when widening the light absorption within the NIR range. The device was realized using NIR fluorescent transparent molecules, in particular cyanines, phthalocyanines and squaraine sensitizers, with the

aim of capturing NIR wavelengths, convert them into visible photons, and subsequently guide them towards the glass edge (where the PV unit was placed) (**Figure 9**). The transparency exhibited by this TLSC was 86%, with a PCE of 0.4%.

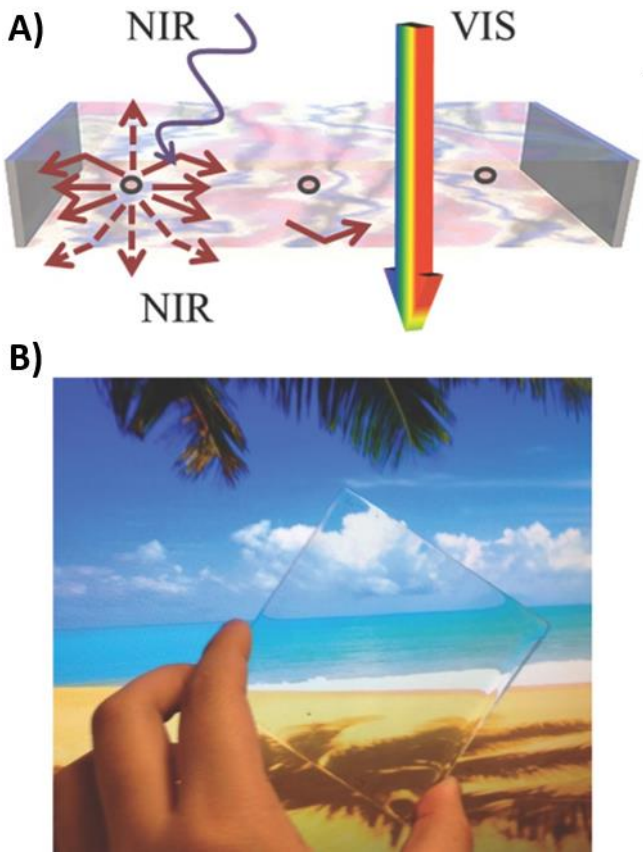

Figure 9. A) Schematic of a TLSC; **B)** Digital picture of a transparent LSC architecture incorporating the cyanine derivative 1-(6-(2,5-dioxopyrrolidin-1-yloxy)-6-oxohexyl)-3,3-dimethyl-2-((E)-2-((E)-3-((E)-2-(1,3,3-trimethylindolin-2-ylidene)ethylidene)cyclohex-1-enyl)vinyl)-3H-indolium chloride as luminophore. Adapted and reprinted with permission from [251].

TLSC can be fabricated also in order to harvest the UV radiation using hexanuclear metal halide in spite of the NIR fluorescent dyes. Also, advanced materials coming from raw sources or design of composites represent a concrete possibility for the next generation of TLSC [252,253,254,255,256,257].

3.3. Overview of the transparent photovoltaic technologies analysed

In order to provide a summarized view of all the examined TPV technologies, **Table 1** displays the comparison between them underling the main electrical and optical aspects according to which they can be classified.

According to what reported above, transparent solar technologies are highly desirable inventions, and can find applications in several environments and daily circumstances, such as in buildings, trains, autovehicles windows, smartphones, laptops, etc. Unfortunately, the processes behind the fabrication of these technologies still face a few obstacles and challenges that the research community is called to overcome:

- The complex choice of compounds that permit the visible wavelengths transmission, and simultaneously allow the harvesting of photons lying in the "invisible" portion of sunlight.
- The scalability of the manufacturing approach adopted for materials preparation behind TPV technologies.
- The most suitable TPV units architecture and the choice of the substrate to be used for device protection.
- The fabrication cost, which must lead to rather cheap products.

To overwhelm the challenges listed in this paragraph, currently active investigations are covering several directions, as listed in **Table 1**. Many among these strategies focus on the search for alternative/unconventional materials able to lead to acceptable transparency levels for particular uses, while different research groups are working on UV or NIR radiation harvesting while transmitting the visible portion of sunlight. However, generally, when the technologies presented above are compared watching at maturity and market closeness, around 80% of them show to be still in the academic investigation phase, needing major improvements so as to become suitable for the PV global market. In such a scenario, investments by multinational companies are urgently required.

Table 1. Comparison among several TPV technologies based on different fabrication processes. *T* denotes the transmission rate percentage of the radiation through the PV unit. Adapted and reprinted with permission from [31].

TPV	**T (%)**	**J_{sc} (mA cm^{-2})**	**V_{oc} (V)**	**FF**	**PCE (%)**	**Ref.**
Screen-printed DSSC	60	16.25	0.779	0.73	9.2	[258]
NIR OPV	55±3	4.7±0.3	0.62±0.02	0.55±0.03	1.7±0.1	[202]
PSC	66	9.3	0.77	56.2	4.02	[259]
TLSC	86±1	1.2±0.1	0.5±0.01	0.66±0.02	0.4±0.03	[251]
PVSC	30	10.30	1.074	57.9	6.4	[229]
Tandem PVSC	77 peak	17.5	1.025	0.71	12.7	[230]

EPD-produced DSSC	55	14.83	0.68	0.71	7.1	[260]
Dip-coated DSSC	≈70	16.17	0.738	0.688	8.22	[261]
QDs solar cell	22.74	12.83	0.58	0.52	3.88	[262]
QDs solar cell	24	0.56	18.2	0.53	5.4	[206]

4. Case study: feasibility analysis of transparent solar cell building integration

Although the vast majority of literature and patent studies are based on experimental or optical approaches, it is important to construct scenarios where transparent technologies are placed in particular environments, in order to study their impact on the overall costs of the building, on the quality of the illuminance and on the payback time (PBT).

The aim of this newly proposed case study is to quantify the capability of semi-TSCs applied to facade and to assess financial effects of the investment. Solar cells are applied as movable blinds to improve building energy performance. The analysis is conducted for each orientation of the building and for three window sizes. The prototype office developed has a square plan of 36 m^2 and is 3.1 m-high. Three window sizes were set during the analysis: 6 m^2, 12 m^2 and 18 m^2. The window is located on the wall adjacent to the external environment, while the other surfaces of the office are considered to be adjoining to conditioned rooms and are, therefore, not subjected to the inter-zonal heat flow. **Figure 10** shows the prototype office room examined. Influences from surrounding buildings, vegetation or other obstructions are disregarded in the simulation.

Figure 10. Digital scheme of the office room designed for the proposed case study.

4.1 Optical and thermal characteristics of the building

The thermal transmittance of opaque surfaces meets the minimum requirement set in the national standards [263] and the visible reflection factors are assumed equal to 50%, 20% and 70% for walls, floor and ceiling, respectively. In order to evaluate thermal and optical properties of the window with and without transparent PV shutters, the software WINDOW 7.7 was used. The reference window was designed with double glass and an air gap in the middle. Optical and thermal characteristics for the glazed surface are summarized in **Table 2**.

Table 2. Optical and thermal characteristics of transparent elements.

	Transparent glass	**PV blinds**	**TG + PV blinds**
Thermal transmittance (W m^{-2} K^{-1})	2.67	1.0	1.93
Visible transmittance	0.8	0.6	0.5
SHGC	0.62	0.42	0.51

Blinds are realized with two semi-transparent PV panels, with each area equal to 0.5 transparent glass area. Movable blinds are used as nocturnal insulation shutter during heating period, their effect is considered by applying a reduced thermal transmittance of window and shutter. Moreover, they are used as solar shading when the incident sunlight on the surface at the given hour is higher than 300 W m^{-2} [264]. When shutters are open, they are supposed to be normal to the facade surface.

4.2 Semi-transparent solar cells and panels configuration

For this analysis it is assumed to install screen-printed DSSCs with an AVT factor of 60% and a PCE equal to 8.7%. The PCE is referred to a single prototype cell, but larger DSSCs are required for large-scale marketing. PV parameters were recalculated according to the relative percentage changes reported by Sygkridoua *et al.* [265].

Each module (10 cm × 30 cm) is realized by connecting 10 cells in series (1 cm × 28 cm). The active area of a module is supposed to be 60% of the total area. Taking into account the cell up-scaling and the lower active area of each module, the total PCE is 7.5%. Panels are connected to an inverter provided with maximum power point tracking system (MPPT).

4.3 Simulation method and conditions

The prototype office is located in Turin (45.070 N, 7.687 E). Weather data, hourly and average monthly solar irradiance are evaluated on a vertical surface for different orientations employing the Photovoltaic Geographical Information System (PVGIS) [266].

The building is occupied every weekday for 10 h, from 8:00 AM to 6:00 PM. The lighting characteristics of the room comply with the requirements imposed by national standards [267]: the maintained illuminance required is 500 lux on the visual task plans and 200 lux in the surrounding areas, respectively. The lighting system chosen for the simulation consists of flat LED panels (electric power of 70 W and luminous efficiency of 113 lm W^{-1}). The Relux simulation software was used to establish the natural and artificial lighting characteristics inside the building and the electricity load required.

Criteria for assessing the building thermal performance are provided by national standards [268]. Heating, cooling and ventilation are activated intermittently, only during office occupation. The set point temperatures are 20 °C for heating and 26 °C for cooling. The air-conditioning unit is powered by a heat pump with an average coefficient of performance (COP) for heating equal to 3.6 and an average energy efficiency ratio (EER) for cooling of 3.2.

The amount of energy generated by solar cells contributes to the reduction of purchased electricity. The energy is produced by the irradiance incident on the photoelectrode. The amount of power produced by the counter electrode is not accounted, underestimating the energy produced. Losses downstream of the PV system such as the inverter, the MPPT and other components are not accounted.

4.4 Outcome of the simulation study

In the economic feasibility analysis of the system it is necessary to evaluate the change of electricity consumption for lighting, heating and cooling, the electricity generation and the investment cost. Results are presented in form of tables and figures: **Figure 11A** shows the change in the energy requirement for heating, cooling and lighting when the PV system is installed, while **Table 3** lists the amount of electricity produced by the PV system. **Figure 11B** presents the net energy saving.

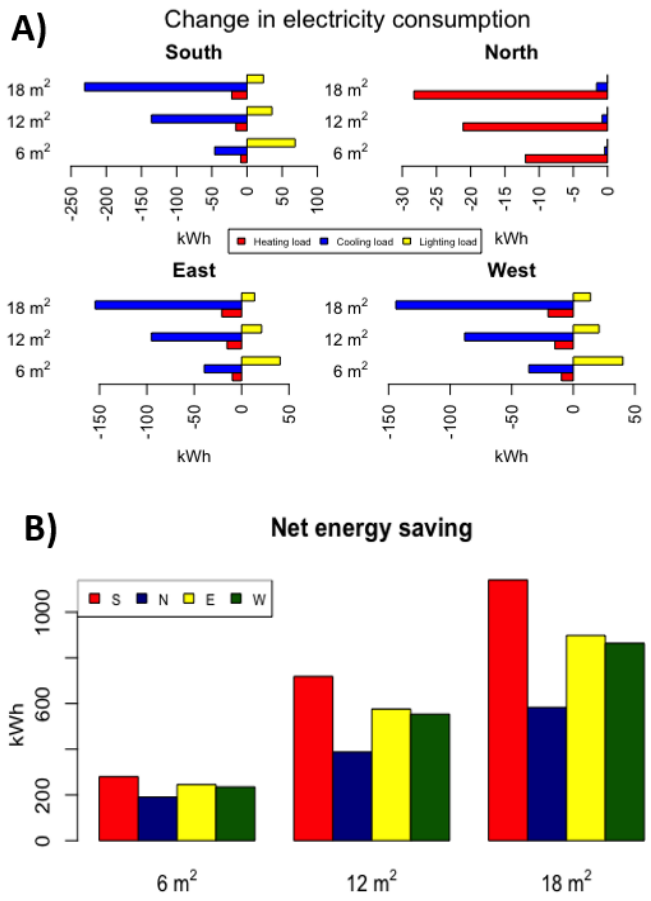

Figure 11. A) Change in electricity consumption when movable blinds are installed; **B)** Net energy saving: sum of the PV energy generation and difference in total energy consumption.

Table 3. Total amount of energy produced per year by PV panels (values expressed in kWh year^{-1}).

	6 m²	**12 m²**	**18 m²**
South	293.4	602.3	911.1
North	178.1	365.6	553.2
East	237.1	486.6	736.2
West	229.6	471.2	712.9

The thermal energy requirements for heating is lower when blinds are installed (from 2% for the smallest window to 9% for the biggest one) since the overall heat transmission coefficient is lower when shutters are closed during the heating season for nocturnal insulation. When the office window is placed towards south, east and west, the cooling load is also reduced (12÷16%) as a result of lower solar heat gain during cooling season when solar shading is in use. Contrariwise, the lighting energy consumption is higher due to lower light transmission coefficient of semi-

transparent solar panels. The rise is more appreciable when the transparent element is facing south (21÷23%) compared to the increment of load at east and west orientation (12÷14%). Instead, when the window is facing north, the effect on cooling and lighting loads is negligible. In fact, blinds are never used as solar shading due to the low incident irradiance on this wall.

The electric power generation is not sufficient to satisfy all the energy needs of the building, but it can still guarantee an energy saving. With a larger window, not only the effect of the screen is enhanced, but also the electricity production of PV panels, clearly, increases. It can provide about 25% of the total load with 6 m^2 PV area. If the transparent surface is higher, the percentage contribution rises remarkably (50% when the area of the window is 12 m^2 and 65% if the size is 18 m^2).

The net energy saving is the balance between the generated electric power and the variation of heating, cooling and lighting energy consumption and it depends on the orientation of the building and on window size. For each area, the highest energy saving occurs with the transparent element south-oriented, while the worst direction is toward north.

The investment cost for the installation of semi-transparent PV panels is 130 € m^{-2} [269]. To assess the economic effect throughout the life of the plant, the net present value (NPV) and the discounted PBT are calculated. **Table 4** and **Table 5** show these results. Both PBT and NPV are more desirable when the window is placed toward south and with the largest size. The higher investment cost is balanced by higher energy saving and higher power generation.

The worst scenario occurs with the glazed surface north-oriented. In this case, both net energy saving and energy generation are low and the initial investment cost is balanced by energy saving after more than 7 years.

Table 4. Net present value after 20 years (values expressed in €).

	South	**North**	**East**	**West**
6 m^2	1037	570	868	813
12 m^2	2891	1157	2145	2027
18 m^2	4654	1733	3383	3204

Table 5. PBT (values expressed in years).

	South	North	East	West
6 m^2	4.75	7.1	5.4	5.7
12 m^2	3.75	7.25	4.75	4.9
18 m^2	3.6	7.25	4.6	4.75

5. A success story of building-integrated photovoltaics: Glass-to-Power

BIPV represents the most concrete final destination for the commercial use of TPVs. **Table 6** shows the electrical and optical features of the four principal PV technologies used in the BIPV scenario. Crystalline silicon modules, bearing the highest PCE, have been found not to be aesthetically appealing. They do not offer any chance of color selection given their intrinsically band-like absorption spectrum. As an alternative, amorphous silicon is optically more homogeneous and visually more comfortable. These aspects make it more suitable for integration as solar windows in new-generation buildings, but it has a really low PCE with respect to its crystalline counterpart. As a possible solution to these issues, PSCs and PVSCs are really emerging as cost-effective choices. They can be printed at high-speed by adopting high-throughput fabrication processes and show relatively high PCE. Moreover, the predicted energy PBT for both organic and perovskite-based PV devices are rapidly decreasing thanks to novel findings in modules fabrication and choice of charge carriers transporting materials, rendering them excellent candidates for power-generating windows.

Table 6. The comparison of electrical and optical features of various kinds of PV cells. Adapted and reprinted with permission from [149].

PV material	Thickness (μm)	Harvesting properties	Charge mobility ($cm^2 V^{-2} s^{-1}$)	Certified PCE (%)
Crystalline Si	300	Broad band Abs. coeff = 10^3	10^3	26.1
Amorphous Si	1	Broad band Abs. coeff = 10^4	10^{-1}	14.0
Perovskite	0.3	Broad band Abs. coeff = 10^5	10^1	25.2
Polymer	0.1	Confined band absorption Abs. coeff = 10^{5-6}	10^{-3}	12.3

In this respect, the Italian company Glass-to-Power has raised 2.25 M€ via crowdfunding to advance its R&D aimed at setup an industrial production line for TSCs [270]. Glass to Power utilizes the LSC technology and aims to reach a PCE of 5%. Photons are guided by total internal reflection to the window edges, and are then transformed into electricity by traditional solar units

mounted along the slab perimeter. The technology behind their LSC panels uses nanoparticles as chromophores, thus decoupling the absorption processes and the emission of light, even in areas of hundreds of square centimeters.

The quality of light transmitted by Glass to Power panels is located in group 1A (UNI 10380 certification), i.e. the group with the highest quality, therefore suitable for lighting houses and offices (**Figure 11A**). Right now, the company declares that it managed to reach PCE values up to 3.2% with a degree of transparency in the visible spectrum of around 80%. Noteworthy, the optical conversion efficiency of the blue/UV fraction of the solar spectrum reaches values exceeding 10% and "ray-tracing" simulations have shown that these performances are also conserved for large-scale units.

Plastic panels behind Glass to Power products are made of high quality Plexiglass (**Figure 11B**), and the nanoparticles used for light-management are made of inorganic materials such as silicon, thus guaranteeing stability under sunlight without any risk of photodegradation of organic components.

The reference market for Glass to Power is that of BIPV for large commercial and residential glass buildings, and its technology also suits in the case of architectural, historical or landscape constraints, contributing to the energy sustainability of existing buildings also where traditional PV cannot be installed. The product is expected to be marketed in 2019 [271].

Figure 11. A) The Glass to Power strategy for LSCs to be integrated in smart building; **B)** Photograph of a Glass to Power panel made of Plexiglass. Adapted and reprinted with permission from [270].

It is conceivable that many other spin-off/company realities like this one will born in the near future, building themselves on the innovation promoted by chemistry and materials science, and with particular inspiration to what the scientific community is studying in the fields of unconventional PV [272,273,274,275,276,277,278]. Besides this, polymer science and technology is making great steps ahead targeting the replacement of oil-derived compounds [279,280,281,282,283], designing new objects by 3D printing [284,285,286,287,288], entering in the Li-ion battery market to achieve lightweight storage pack units [289,290,291,292] and, last but not least, offering novel biomedical devices bearing high compatibility with human organisms and long-term stability [293,294,295,296]. On the other hand, chemical sciences are re-starting to explore inorganic materials, especially for those applications where stability under radiation and thermal aging are concrete problems for organic matrix systems [297,298,299,300,301]. In this scenario, new semiconductor nanostructures and composite materials containing different inorganic compounds are emerging and providing important responses in the fields of energy and environment [302,303,304,305,306,307].

The transition from micro to nano has pervaded the sciences in the past twenty years, but only today are we are started enjoying nanotechnologies [308,309,310,311,312]. Among these, the PV field counts several applications and the scientific community is working towards new integrations with systems for CO_2 reduction and decontamination of waste water [313,314,315,316,317]. Furthermore, nanoscience field includes a new generation of sensors, where highly responsive nanostructures are able to monitor traces of chemical species at a very low concentration [318,319,320,321,322]. In any case, the field of nanoscience will remain closely linked to that of the sustainability of materials and processes. The novel PV technologies (and the energy field in general) must be based on abundant materials [323,324,325,326,327], not impacting on the ecosystem and, possibly, reusable at the end of their life [328,329,330,331]. To this end, the training of new generations of scientists is important and some recent publications are showing interesting advanced to this purpose [332,333,334,335,336].

In summary, scientists today can make use of cutting edge, advanced synthesis techniques. Among the salient aspects, a nanomaterial developed for a certain application can also be used for other purposes: PV includes several compounds capable of interacting with sunlight or transporting charges that are used or can be used even in other (also very different) fields [337,338,339,340]. To this purpose, chemical synthesis remains a cornerstone of the technological development, for which the ability to design molecules to meet today's energy needs is priceless [341,342,343,344].

6. Conclusions

Highly transparent PVs represents a valid possibility to substantially offset fossils fuel consumption worldwide. Their effective commercialization and widespread adoption require the mutual optimization of PCE and AVT. The challenge is given by the intrinsic conflict between transparency and light harvesting concepts.

This manuscript has reviewed several technologies for TPVs, all of them having achieved transmission levels higher than 20%. They were classified according to different approaches to reach high transparency levels along with the highest possible PCE, also highlighting the big challenges that need to be faced in order to turn them into realisable technologies. Among transparent, segmented and thin-film solar cells it emerged that the former are the most credible towards a truly efficiency transparent PV concept, and will surely be of interest of several companies in the near future. As an alternative, solar concentrators could offer valid performances,

e.g. PCE = 5% and AVT = 50-60%, simplifying the window fabrication and installation in several circumstancies.

In order to provide a practical application of TPVs, a case study simulating a real office in Europe has been proposed and analyzed in terms of energy, environmental and financial issues. The electric power generation is not sufficient to satisfy all the energy needs of the building, but it can still guarantee an energy saving; the overall PBT is 3.6 years with South exposition.

A comparison between optical and electrical properties offered by amorphous silicon panels and recently emerged semi-transparent technologies has also been proposed, such as PSCs and PVSCs, highlighting the valuable impact that TPVs can have in the BIPVs market. Focusing on this consideration, the case of a start-up company in Italy, i.e. Glass to Power, which has recently crowdfunded 2.25 M€ to advance its plans for the set-up of an industrial production line of LSCs to be used in windows applications for buildings, has been reported.

Acknowledgements

This research did not receive any specific grant from funding agencies in the public, commercial, or not-for-profit sectors.

References

[1] Chu S, Majumdar A. Opportunities and challenges for a sustainable energy future. Nature 2012;488:294-303.

[2] Eslami S, Gholami A, Bakhtiari A, Zandi M, Noorollahi Y. Experimental investigation of a multi-generation energy system for a nearly zero-energy park: A solution toward sustainable future. Energy Convers Manage 2019;200:112107.

[3] Kılkış Ş, Krajačić G, Duić N, Montorsi L, Wang Q, Rosen MA, Ahmad Al-Nimr M. Research frontiers in sustainable development of energy, water and environment systems in a time of climate crisis. Energy Convers Manage 2019;199:111938.

[4] Whiting K, Carmona LG, Carrasco A, Sousa T. Exergy replacement cost of fossil fuels: Closing the carbon cycle. Energies 2017;10:979.

[5] Kotilainen K, Saari UA, Mäkinen SJ, Ringle CM. Exploring the microfoundations of end-user interests toward co-creating renewable energy technology innovations. J Cleaner Prod 2019;229:203-12.

[6] Østergaard PA, Duic N, Noorollahi Y, Mikulcic H, Kalogirou S. Sustainable development using renewable energy technology. Renewable Energy 2020;146:2430-7.

[7] Wang JC, Liao MS, Lee YC, Liu CY, Kuo KC, Chou CY, Huang CK, Jiang JA. On enhancing energy harvesting performance of the photovoltaic modules using an automatic cooling system and assessing its economic benefits of mitigating greenhouse effects on the environment. J Power Sources 2018;376:55-65.

[8] Gavriluta A, Fix T, Nonat A, Slaoui A, Guillemoles JF, Charbonnière LJ. Eu^{III}-based nanolayers as highly efficient downshifters for CIGS solar cells. Eur J Inorg Chem 2017; 2017:5318-26.

[9] Siddiqui FY, Shaikh SU, Upadhye DS, Huse NP, Dive AS, Sharma R. Investigation on the effect of copper doping on $CdS_{1-x}Se_x$ thin films. Ferroelectrics 2017;518:153-62.

[10] Manwell JF, McGowan JG, Breger D. A design and analysis tool for utility scale power systems incorporating large scale wind, solar photovoltaics and energy storage. J Storage Mater 2018;19:103-12.

[11] Mito MT, Ma X, Albuflasa H, Davies PA. Reverse osmosis (RO) membrane desalination driven by wind and solar photovoltaic (PV) energy: State of the art and challenges for large-scale implementation. Renewable Sustainable Energy Rev 2019;112:669-85.

[12] Kim T, Kim JH, Triambulo RE, Han H, Park C, Park JW. Improving the stability of organic–inorganic hybrid perovskite light-emitting diodes using doped electron transport materials. Phys Status Solidi A 2019;216:1900426.

[13] Kim JY, Baek W, Kim S, Kang G, Han IK, Hyeon T, Park M. Moisture proof hole transport layers based on CISe quantum dots for highly stable and large active area perovskite solar cells. Appl Surf Sci 2019;496:143610.

[14] Abdelhamid HN, El-Zohry AM, Cong J, Thersleff T, Karlsson M, Kloo L, Zou X. Towards implementing hierarchical porous zeolitic imidazolate frameworks in dye-sensitized solar cells. R Soc Open Sci 2019;6:190723.

[15] Ming B, Liu P, Guo S, Cheng L, Zhang J. Hydropower reservoir reoperation to adapt to large-scale photovoltaic power generation. Energy 2019;179:268-79.

[16] Umar A, Akhtar MS, Almas T, Ibrahim AA, Al-Assiri MS, Masuda Y, Rahman QI, Baskoutas S. Direct growth of flower-shaped ZnO nanostructures on FTO substrate for dye-sensitized solar cells. Crystals 2019;9:405.

[17] Qiu L, He S, Ono LK, Liu S, Qi Y. Upscalable fabrication of metal halide perovskite solar cells and modules. ACS Energy Lett 2019;4:2147-67.

[18] Falk LM, Goetz KP, Lami V, An Q, Fassl P, Herkel J, Thome F, Taylor AD, Paulus F, Vaynzof Y. Effect of precursor stoichiometry on the performance and stability of $MAPbBr_3$ photovoltaic devices. Energy Technol 2020;8:1900737.

[19] Saidi NM, Omar FS, Numan A, Apperley DC, Algaradah MM, Kasi R, Avestro AJ, Subramaniam RT. Enhancing the efficiency of a dye-sensitized solar cell based on a metal oxide nanocomposite gel polymer electrolyte. ACS Appl Mater Interfaces 2019;11:30185-96.

[20] Traverse CJ, Pandey R, Barr MC, Lunt RR. Emergence of highly transparent photovoltaics for distributed applications. Nat Energy 2017;2:849-60.

[21] Halme J, Mäkinen P. Theoretical efficiency limits of ideal colored opaque photovoltaics. Energy Environ Sci 2019;12:1274-85.

[22] Lunt RR. Theoretical limits for visibly transparent photovoltaics. Appl Phys Lett 2012;101:043902.

[23] Saretta E, Caputo P, Frontini F. A review study about energy renovation of building facades with BIPV in urban environment. Sustain Cities Soc 2019;44:343-55.

[24] Zhang T, Wang M, Yang H. A review of the energy performance and life-cycle assessment of building-integrated photovoltaic (BIPV) systems. Energies 2018;11:3157.

[25] Shukla AK, Sudhakar K, Baredar P, Mamat R. Solar PV and BIPV system: Barrier, challenges and policy recommendation in India. Renewable Sustainable Energy Rev 2018;82:3314-22.

[26] Guo X, Koh TM, Febriansyah B, Han G, Bhaumik S, Li J, Jamaludin NF, Ghosh B, Chen X, Mhaisalkar S, Mathews N. Cesium oleate passivation for stable perovskite photovoltaics. ACS Appl Mater Interfaces 2019;11:27882-9.

[27] Kapil G, Bessho T, Ng CH, Hamada K, Pandey M, Kamarudin MA, Hirotani D, Kinoshita T, Minemoto T, Shen Q, Toyoda T, Murakami TN, Segawa H, Hayase S. Strain relaxation and light management in tin-lead perovskite solar cells to achieve high efficiencies. ACS Energy Lett 2019;4:1991-8.

[28] Chou YS, Chou LH, Guo AZ, Wang XF, Osaka I, Wu CG, Liu CL. Ultrasonic spray-coated mixed cation perovskite films and solar cells. ACS Sustainable Chem Eng 2019;7:14217-24.

[29] Mohamad AA. Physical properties of quasi-solid-state polymer electrolytes for dye-sensitised solar cells: A characterisation review. Sol Energy 2019;190:434-52.

[30] Liu Y, Zhang Z, Gao H, Zhang H, Mao Y. A novel inorganic hole-transporting material of $CuInS_2$ for perovskite solar cells with high efficiency and improved stability. Org Electron 2019;75:105430.

[31] Husain AAF, Hasan WZW, Shafie S, Hamidon MN, Pandey SS. A review of transparent solar photovoltaic technologies. Renewable Sustainable Energy Rev 2018;94:779-91.

[32] Zhang N, Chen G, Xu Y, Xu X, Yu L. Power generation, evaporation mitigation, and thermal insulation of semitransparent polymer solar cells: A potential for floating photovoltaic applications. ACS Appl Energy Mater 2019;2:6060-70.

[33] Acciari G, Adamo G, Ala G, Busacca A, Caruso M, Giglia G, Imburgia A, Livreri P, Miceli R, Parisi A, Pellitteri F, Pernice R, Romano P, Schettino G, Viola F. Experimental investigation on the performances of innovative PV vertical structures. Photonics 2019;6:86.

[34] Chen S, Solanki A, Pan J, Sum TC. Compositional and morphological changes in water-induced early-stage degradation in lead halide perovskites. Coatings 2019;9:535.

[35] Zhang WX, Lin ZX, Huang R, Guo Y. Effect of phase transition on optical properties and photovoltaic performance in cesium lead bromine perovskite: A theoretical study. J Phys Chem C 2019;123:20764-8.

[36] Yoo GY, Azmi R, Kim C, Kim W, Min BK, Jang SY, Do YR. Stable and colorful perovskite solar cells using a nonperiodic SiO_2/TiO_2 multi-nanolayer filter. ACS Nano 2019;13:10129-39.

[37] Li B, Fu L, Li S, Li H, Pan L, Wang L, Chang B, Yin L. Pathways toward high-performance inorganic perovskite solar cells: Challenges and strategies. J Mater Chem A 2019;7:20494-518.

[38] Yang JA, Qin T, Xie L, Liao K, Li T, Hao F. Methylamine-induced defect-healing and cationic substitution: A new method for low-defect perovskite thin films and solar cells. J Mater Chem C 2019;7:10724-42.

[39] Liu Y, Chen C, Zhou Y, Kondrotas R, Tang J. Butyldithiocarbamate acid solution processing: Its fundamentals and applications in chalcogenide thin film solar cells. J Mater Chem C 2019;7:11068-84.

[40] Ahmad Z, Aziz F, Abdullah HY. Study on the stability of the mixed ($MAPbI_3$ and $MAPbBr_3$) perovskite solar cells using dopant-free HTL. Org Electron 2020;76:105453.

[41] Olympus Corporation, https://www.olympus-lifescience.com/en/microscope-resource/primer/java/solarcell/, accessed May 2020.

[42] Wright IA. Phosphorescent molecular metal complexes in heterojunction solar cells. Polyhedron 2018;140:84-98.

[43] Duan SN, Dall'Agnese C, Ojima H, Wang XF. Effect of solvent-induced phase separation on performance of carboxylic indoline-based small-molecule organic solar cells. Dyes Pigm 2018;151:110-5.

[44] Wang JC, Hill SP, Dilbeck T, Ogunsolu OO, Banerjee T, Hanson K. Multimolecular assemblies on high surface area metal oxides and their role in interfacial energy and electron transfer. Chem Soc Rev 2018;47:104-48.

[45] Saaid FI, Tseng TY, Winie T. Effect of ionic liquid concentration on the photovoltaic performance of dye-sensitized solar cell. Mater Today Proc 2019;17:401-7.

[46] Koyyada G, Chitumalla RK, Thogiti S, Kim JH, Jang J, Chandrasekharam M, Jung JH. A new series of EDOT based co-sensitizers for enhanced efficiency of cocktail DSSC: A comparative study of two different anchoring groups. Molecules 2019;24:3554.

[47] Li Y, Lin H, Zeng J, Chen J, Chen H. Enhance short-wavelength response of CIGS solar cell by CdSe quantum disks as luminescent down-shifting material. Sol Energy 2019;193:303-8.

[48] Liang Q, Qiao F, Yang J, Jiang Y, Xu Q, Wang Q. Present research status and progress of solar cells. Mater China 2019;38:505-11.

[49] Lei L, Yang S, Yu Y, Li M, Xie J, Bao S, Jin P, Huang A. Long-term stable perovskite solar cells with room temperature processed metal oxide carrier transporters. J Mater Chem A 2019;7:21085-95.

[50] Singh J, Agrahari A. The progression of silicon technology acting as substratum for the betterment of future photovoltaics. Int J Energy Res 2019;43:3959-80.

[51] Wetzel T, Borchers S. Update of energy payback time and greenhouse gas emission data for crystalline silicon photovoltaic modules. Prog Photovoltaics Res Appl 2015;23:1429-35.

[52] Yang Z, Song J, Zeng H, Wang M. Organic composition tailored perovskite solar cells and light-emitting diodes: Perspectives and advances. Mater Today Energy 2019;14:100338.

[53] Oh WC, Areerob Y. A new aspect for band gap energy of graphene-$Mg_2CuSnCoO_6$-gallic acid as a counter electrode for enhancing dye-sensitized solar cell performance. ACS Appl Mater Interfaces 2019;11:38859-67.

[54] Zheng J, Mehrvarz H, Liao C, Bing J, Cui X, Li Y, Gonçales VR, Lau CFJ, Lee DS, Li Y, Zhang M, Kim J, Cho Y, Caro LG, Tang S, Chen C, Huang S, Ho-Baillie AWY. Large-area 23%-efficient monolithic perovskite/homojunction-silicon tandem solar cell with enhanced UV stability using down-shifting material. ACS Energy Lett 2019;4:2623-31.

[55] Chuang TK, Anuratha KS, Lin JY, Huang KC, Su CH, Hsieh CK. Low temperature growth of carbon nanotubes using chemical bath deposited $Ni(OH)_2$ – An efficient Pt-free counter electrodes for dye-sensitized solar cells. Surf Coat Technol 2018;344:534-40.

[56] Hu J, Kontos AG, Georgiou CA, Bidikoudi M, Stein N, Breen B, Falaras P. Combining dc and ac electrochemical characterization with micro Raman analysis on industrial DSCs under accelerated thermal stress. Electrochim Acta 2018;271:268-75.

[57] Venkatraman V, Raju R, Oikonomopoulos SP, Alsberg BK. The dye-sensitized solar cell database. J Cheminf 2018;10:18.

[58] Xie Y, Gao J, Zhang S, Wu L. Novel indeno[2,1-b] carbazole donor-based organic dyes for dye-sensitized solar cells. Photochem Photobiol Sci 2018;17:423-31.

[59] Zhang J, Lou Y, Liu M, Zhou H, Zhao Y, Wang Z, Shi L, Li D, Yuan S. High-performance dye-sensitized solar cells based on colloid-solution deposition planarized fluorine-doped tin oxide substrates. ACS Appl Mater Interfaces 2018;10:15697-703.

[60] Cacovich S, Matteocci F, Abdi-Jalebi M, Stranks SD, Di Carlo A, Ducati C, Divitini G. Unveiling the chemical composition of halide perovskite films using multivariate statistical analyses. ACS Appl Energy Mater 2018;1:7174-81.

[61] Schlipf J, Hu Y, Pratap S, Bießmann L, Hohn N, Porcar L, Bein T, Docampo P, Müller-Buschbaum P. Shedding light on the moisture stability of 3D/2D hybrid perovskite heterojunction thin films. ACS Appl Energy Mater 2019;2:1011-8.

[62] Yang TY, Jeon NJ, Shin HW, Shin SS, Kim YY, Seo J. Achieving long-term operational stability of perovskite solar cells with a stabilized efficiency exceeding 20% after 1000 h. Adv Sci 2019;6:1900528.

[63] Di Girolamo D, Dar MI, Dini D, Gontrani L, Caminiti R, Mattoni A, Graetzel M, Meloni S. Dual effect of humidity on cesium lead bromide: Enhancement and degradation of perovskite films. J Mater Chem A 2019;7:12292-302.

[64] Yu X, Yan H, Peng Q. Reaction temperature and partial pressure induced etching of methylammonium lead iodide perovskite by trimethylaluminum. Langmuir 2019;35:6522-31.

[65] Rajan AK, Cindrella L. Studies on new natural dye sensitizers from Indigofera tinctoria in dye-sensitized solar cells. Opt Mater 2019;88:39-47.

[66] Jia HL, Peng ZJ, Chen YC, Huang CY, Guan MY. Highly efficient stereoscopic phenothiazine dyes with different anchors for dye-sensitized solar cells. New J Chem 2018;42: 18702-7.

[67] Guo SW, Sun YR, Qi JB, Zheng Y, Zhang QH. Preparation and characterization of dye-sensitized solar cells by liquid phase deposition method at low temperature. J Synth Cryst 2017;46:2326-31.

[68] Rajan AK, Cindrella L. Potential of aldehyde bearing N,N-diphenylhydrazone based organic dye in TiO_2, ZnO and TiO_2/ZnO bilayer semiconductor constituting dye sensitized solar cells. Mater Res Express 2019;6:0850E6.

[69] Manzoor T, Pandith AH. Enhancing the photoresponse by CdSe-Dye-TiO_2-based multijunction systems for efficient dye-sensitized solar cells: A theoretical outlook. J Comput Chem 2019;40:2444-52.

[70] Piana G, Ricciardi M, Bella F, Cucciniello R, Proto A, Gerbaldi C. Poly(glycidyl ether)s recycling from industrial waste and feasibility study of reuse as electrolytes in sodium-based batteries. Chem Eng J 2020;382:122934.

[71] Piana G, Bella F, Geobaldo F, Meligrana G, Gerbaldi C. PEO/LAGP hybrid solid polymer electrolytes for ambient temperature lithium batteries by solvent-free, "one pot" preparation. J Energy Storage 2019;26:100947.

[72] Falco M, Simari C, Ferrara C, Nair JR, Meligrana G, Bella F, Nicotera I, Mustarelli P, Winter M, Gerbaldi C. Understanding the effect of UV-induced cross-linking on the physicochemical properties of highly performing PEO/LiTFSI-based polymer electrolytes. Langmuir 2019;35:8210-9.

[73] Nair JR, Colò F, Kazzazi A, Moreno M, Bresser D, Lin R, Bella F, Meligrana G, Fantini S, Simonetti E, Appetecchi GB, Passerini S, Gerbaldi C. Room temperature ionic liquid (RTIL)-based electrolyte cocktails for safe, high working potential Li-based polymer batteries. J Power Sources 2019;412:398-407.

[74] Falco M, Castro L, Nair JR, Bella F, Bardé F, Meligrana G, Gerbaldi C. UV-cross-linked composite polymer electrolyte for high-rate, ambient temperature lithium batteries. ACS Appl Energy Mater 2019;2:1600-7.

[75] Scalia A, Bella F, Lamberti A, Gerbaldi C, Tresso E. Innovative multipolymer electrolyte membrane designed by oxygen inhibited UV-crosslinking enables solid-state in plane integration of energy conversion and storage devices. Energy 2019;166:789-95.

[76] Lefrançois Perreault L, Colò F, Meligrana G, Kim K, Fiorilli S, Bella F, Nair JR, Vitale-Brovarone C, Florek J, Kleitz F, Gerbaldi C. Spray-dried mesoporous mixed Cu-Ni oxide@graphene nanocomposite microspheres for high power and durable Li-ion battery anodes. Adv Energy Mater 2018;8:1802438.

[77] Suriyakumar S, Gopi S, Kathiresan M, Bose S, Gowd EB, Nair JR, Angulakshmi N, Meligrana G, Bella F, Gerbaldi C, Stephan AM. Metal organic framework laden poly(ethylene

oxide) based composite electrolytes for all-solid-state Li-S and Li-metal polymer batteries. Electrochim Acta 2018;285:355-64.

[78] Bella F, Muñoz-García AB, Colò F, Meligrana G, Lamberti A, Destro M, Pavone M, Gerbaldi C. Combined structural, chemometric, and electrochemical investigation of vertically aligned TiO_2 nanotubes for Na-ion batteries. ACS Omega 2018;3:8440-50.

[79] Radzir NNM, Hanifah SA, Ahmad A, Hassan NH, Bella F. Effect of lithium bis(trifluoromethylsulfonyl)imide salt-doped UV-cured glycidyl methacrylate. J Solid State Electrochem 2015;19:3079-85.

[80] Zolin L, Nair JR, Beneventi D, Bella F, Destro M, Jagdale P, Cannavaro I, Tagliaferro A, Chaussy D, Geobaldo F, Gerbaldi C. A simple route toward next-gen green energy storage concept by nanofibres-based self-supporting electrodes and a solid polymeric design. Carbon 2016;107:811-22.

[81] Grätzel M. Dye-sensitized solar cells. J. Photochem Photobiol, C 2003;4:145-53.

[82] Prabakaran K, Jandas PJ, Mohanty S, Nayak SK. Synthesis, characterization of reduced graphene oxide nanosheets and its reinforcement effect on polymer electrolyte for dye sensitized solar cell applications. Sol Energy 2018;170:442-53.

[83] Popoola IK, Gondal MA, AlGhamdi JM, Qahtan TF. Photofabrication of highly transparent platinum counter electrodes at ambient temperature for bifacial dye sensitized solar cells. Sci Rep 2018;8:12864.

[84] Chen R, Weng Q, An Z, Zhu S, Wang Q, Chen X, Chen P. Investigation of 4-pyridyl liquid crystals on the photovoltaic performance and stability of dye sensitized solar cells by the co-sensitization. Dyes Pigm 2018;159:527-32.

[85] Saygili Y, Stojanovic M, Flores-Díaz N, Zakeeruddin SM, Vlachopoulos N, Grätzel M, Hagfeldt A. Metal coordination complexes as redox mediators in regenerative dye-sensitized solar cells. Inorganics 2019;7:30.

[86] Dhar A, Kumar NS, Asif M, Vekariya RL. Systematic study of mono- and tri-TEMPO-based electrolytes for highly efficient next-generation dye-sensitised photo harvesting. J Photochem Photobiol, A 2018;363:1-6.

[87] Oh J, Ghann W, Kang H, Nesbitt F, Providence S, Uddin J. Comparison of the performance of dye sensitized solar cells fabricated with ruthenium based dye sensitizers: Di-tetrabutylammonium cis-bis(isothiocyanato)bis(2,2'-bipyridyl-4,4'-dicarboxylato)ruthenium(II) (N719) and tris(bipyridine)ruthenium(II) chloride (Ru-BPY). Inorg Chim Acta 2018;482:943-50.

[88] Peddapuram A, Cheema H, McNamara LE, Zhang Y, Hammer NI, Delcamp JH. Quinoxaline-based dual donor, dual acceptor organic dyes for dye-sensitized solar cells. Appl Sci 2018;8:1421.

[89] Sen A, Groß A. Promising sensitizers for dye sensitized solar cells: A comparison of Ru(II) with other earth's scarce and abundant metal polypyridine complexes. Int J Quantum Chem 2019;119:e25963.

[90] Ghann W, Sharma V, Kang H, Karim F, Richards B, Mobin SM, Uddin J, Rahman MM, Hossain F, Kabir H, Uddin N. The synthesis and characterization of carbon dots and their application in dye sensitized solar cell. Int J Hydrogen Energy 2019;44:14580-7.

[91] Ma P, Lu W, Yan X, Li W, Li L, Fang Y, Yin X, Liu Z, Lin Y. Heteroatom tri-doped porous carbon derived from waste biomass as Pt-free counter electrode in dye-sensitized solar cells. RSC Adv 2018;8:18427-33.

[92] Jia HL, Peng ZJ, Guan MY. New porphyrin dyes containing a hydrazide anchor for dye-sensitized solar cells. New J Chem 2018;42:13770-4.

[93] Naresh Kumar P, Sakthivel K, Balasubramanian V, Sengottaiyan D, Suresh J. Microwave assisted green synthesis of ZnO nanorods for dye sensitized solar cell application. Indian J Chem Technol 2018;25:383-9.

[94] Cole JM, Pepe G, Al Bahri OK, Cooper CB. Cosensitization in dye-sensitized solar cells. Chem Rev 2019;119:7279-327.

[95] Capasso A, Bellani S, Palma AL, Najafi L, Del Rio Castillo AE, Curreli N, Cina L, Miseikis V, Coletti C, Calogero G, Pellegrini V, Di Carlo A, Bonaccorso F. CVD-graphene/graphene flakes dual-films as advanced DSSC counter electrodes. 2D Mater 2019;6:035007.

[96] Jiang R, Boschloo G. The impact of non-uniform photogeneration on mass transport in dye-sensitised solar cells. J Mater Chem A 2018;6:10264-76.

[97] Siwach B, Mohan D, Singh KK, Kumar A, Barala M. Effect of carbonaceous counter electrodes on the performance of ZnO-graphene nanocomposites based dye sensitized solar cells. Ceram Int 2018;44:21120-6.

[98] Kesavan M, Arulraj A, Rajendran K, Anbarasu P, Ganesh PA, Jeyakumar D, Ramesh M. Performance of dye-sensitized solar cells employing polymer gel as an electrolyte and the influence of nano-porous materials as fillers. Mater Res Express 2018;5:115305.

[99] Chiang CT, Chien LY. A Pitaya dye-sensitized solar cell monitor for environmental sunlight intensity detection. IEEE Sens J 2019;19:4229.

[100] Mazloum-Ardakani M, Arazi R, Mirjalili BBF, Azad S. Synthesis and application of Fe_3O_4@nanocellulose/TiCl as a nanofiller for high performance of quasisolid-based dye-sensitized solar cells. Int J Energy Res 2019;43:4483-94.

[101] Shanti R, Bella F, Salim YS, Chee SY, Ramesh S, Ramesh K. Poly(methyl methacrylate-co-butyl acrylate-co-acrylic acid): Physico-chemical characterization and targeted dye sensitized solar cell application. Mater Des 2016;108:560-9.

[102] Bella F, Verna A, Gerbaldi C. Patterning dye-sensitized solar cell photoanodes through a polymeric approach: A perspective. Mater Sci Semicond Process 2018;73:92-8.

[103] Pugliese D, Lamberti A, Bella F, Sacco A, Bianco S, Tresso E. TiO_2 nanotubes as flexible photoanode for back-illuminated dye-sensitized solar cells with hemi-squaraine organic dye and iodine-free transparent electrolyte. Org Electron 2014;15:3715-22.

[104] Çakar S, Özacar M. The pH dependent tannic acid and Fe-tannic acid complex dye for dye sensitized solar cell applications. J Photochem Photobiol, A 2019;371:282-91.

[105] Soonmin H, Shanmugam M, Mordiya M, Markna JH. Review on dye-sensitized solar cells based on polymer electrolytes. Int J Res Eng Technol 2018;7:3001-6.

[106] Rai P. Plasmonic noble metal@metal oxide core-shell nanoparticles for dye-sensitized solar cell applications. Sustainable Energy Fuels 2019;3:63-91.

[107] Pujiarti H, Bahar H, Hidayat R. Poly(ionic-liquid) from imidazoline-functionalized siloxane prepared by simple sol-gel route for efficient quasi-solid-state DSSC. Mater Res Express 2019;6:075507.

[108] Bella F, Galliano S, Piana G, Giacona G, Viscardi G, Grätzel M, Barolo C, Gerbaldi C. Boosting the efficiency of aqueous solar cells: A photoelectrochemical estimation on the effectiveness of $TiCl_4$ treatment. Electrochim Acta 2019;302:31-7.

[109] Pugliese D, Bella F, Cauda V, Lamberti A, Sacco A, Tresso E, Bianco S. A chemometric approach for the sensitization procedure of ZnO flowerlike microstructures for dye-sensitized solar cells. ACS Appl Mater Interfaces 2013;5:11288-95.

[110] Miccoli B, Cauda V, Bonanno A, Sanginario A, Bejtka K, Bella F, Fontana M, Demarchi D. One-dimensional ZnO/gold junction for simultaneous and versatile multisensing measurements. Sci Rep 2016;6:29763.

[111] Imperiyka M, Ahmad A, Hanifah SA, Bella F. A UV-prepared linear polymer electrolyte membrane for dye-sensitized solar cells. Physica B 2014;450:151-4.

[112] Bella F, Lamberti A, Sacco A, Bianco S, Chiodoni A, Bongiovanni R. Novel electrode and electrolyte membranes: Towards flexible dye-sensitized solar cell combining vertically aligned TiO_2 nanotube array and light-cured polymer network. J Membr Sci 2014;470:125-31.

[113] Bella F, Popovic J, Lamberti A, Tresso E, Gerbaldi C, Maier J. Interfacial effects in solid-liquid electrolytes for improved stability and performance of dye-sensitized solar cells. ACS Appl Mater Interfaces 2017;9:37797-803.

[114] Boldrini CL, Manfredi N, Perna FM, Capriati V, Abbotto A. Designing eco-sustainable dye-sensitized solar cells by the use of a menthol-based hydrophobic eutectic solvent as an effective electrolyte medium. Chem Eur J 2018;24:17656-9.

[115] Li G, Sheng L, Li T, Hu J, Li P, Wang K. Engineering flexible dye-sensitized solar cells for portable electronics. Sol Energy 2019;177:80-98.

[116] Benesperi I, Michaels H, Freitag M. The researcher's guide to solid-state dye-sensitized solar cells. J Mater Chem C 2018;6:11903-42.

[117] Nonomura K, Vlachopoulos N, Unger E, Häggman L, Hagfeldt A, Boschloo G. Blocking the charge recombination with diiodide radicals by TiO_2 compact layer in dye-sensitized solar cells. J Electrochem Soc 2019;166:B3203-8.

[118] Liu IP, Wang LW, Tsai MH, Chen YY, Teng H, Lee YL. A new mechanism for interpreting the effect of TiO_2 nanofillers in quasi-solid-state dye-sensitized solar cells. J Power Sources 2019;433:226693.

[119] Carella A, Borbone F, Centore R. Research progress on photosensitizers for DSSC. Front Chem 2018;6:481.

[120] Ramar A, Chen TW, Chen SM, Mutharasu D, Rwei SP. Photoelectrochemical effect of poly(N-vinylcarbazole) as electrolyte additive in a N719 dye sensitized TiO_2 solar cell. Int J Electrochem Sci 2018;13:9721-30.

[121] Kesavan M, Arulraj A, Sannasi V, Rajendran K, Anbarasu P, Jeyakumar D, Ramesh M. Performance of cross-linked polymers based gel electrolyte in the fabrication of quasi-solid state dye-sensitized solar cells. Mater Res Innovations 2020;24:1.

[122] Buene AF, Boholm N, Hagfeldt A, Hoff BH. Effect of furan p-spacer and triethylene oxide methyl ether substituents on performance of phenothiazine sensitizers in dye-sensitized solar cells. New J Chem 2019;43:9403-10.

[123] Kaschuk JJ, Miettunen K, Borghei M, Frollini E, Rojas OJ. Electrolyte membranes based on ultrafine fibers of acetylated cellulose for improved and long-lasting dye-sensitized solar cells. Cellulose 2019;26:6151-63.

[124] Bella F, Sacco A, Massaglia G, Chiodoni A, Pirri CF, Quaglio M. Dispelling clichés at the nanoscale: the true effect of polymer electrolytes on the performance of dye-sensitized solar cells. Nanoscale 2015;7:12010-7.

[125] Bella F, Chiappone A, Nair JR, Meligrana G, Gerbaldi C. Effect of different green cellulosic matrices on the performance of polymeric dye-sensitized solar cells. Chem Eng Trans 2014;41:211-6.

[126] Pintossi D, Iannaccone G, Colombo A, Bella F, Välimäki M, Väisänen KL, Hast J, Levi M, Gerbaldi C, Dragonetti C, Turri S, Griffini G. Luminescent downshifting by photo-induced sol-gel hybrid coatings: Accessing multifunctionality on flexible organic photovoltaics via ambient temperature material processing. Adv Electron Mater 2016;2:1600288.

[127] Bella F, Ozzello ED, Sacco A, Bianco S, Bongiovanni R. Polymer electrolytes for dye-sensitized solar cells prepared by photopolymerization of PEG-based oligomers. Int. J. Hydrogen Energy 2014;39:3036-45.

[128] Bella F, Imperiyka M, Ahmad A. Photochemically produced quasi-linear copolymers for stable and efficient electrolytes in dye-sensitized solar cells. J Photochem Photobiol, A 2014;289:73-80.

[129] Ngidi NPD, Ollengo MA, Nyamori VO. Heteroatom-doped graphene and its application as a counter electrode in dye-sensitized solar cells. Int J Energy Res 2018;43:1702-34.

[130] Tao L, Zhang W, Wang Z, Wang H, Zhang J, Huo Z, Dai S, Hayat T, Alharbi NS. Highly improved photocurrent and stability of dye-sensitized solar cell through quasi-solid-state electrolyte formed by two low molecular mass organogelators. Org Electron 2019;65:179-84.

[131] Mamat S, Faizzi M, Sukor Su'ait M, Ahmad Ludin N, Sopian K, Dzulkurnain NA, Ahmad A, Shyuan LK, Khoon LT, Brandell D. An investigation of modified natural rubber-based (MG49) polymer electrolyte in dye-sensitized solar cells. Sains Malaysiana 2018;47:2667-76.

[132] Çakar S. 1,10 phenanthroline 5,6 diol metal complex (Cu, Fe) sensitized solar cells: A cocktail dye effect. J Power Sources 2019;435:226825.

[133] Yogananda KC, Ramasamy E, Vasantha Kumar S, Rangappa D. Synthesis, characterization, and dye-sensitized solar cell fabrication using potato starch– and potato starch nanocrystal–based gel electrolytes. Ionics 2019;25:6035-42.

[134] Huang Y, Chen WC, Zhang XX, Ghadari R, Fang XQ, Yu T, Kong FT. Ruthenium complexes as sensitizers with phenyl-based bipyridine anchoring ligands for efficient dye-sensitized solar cells. J Mater Chem C 2018;6:9445-52.

[135] Akula SB, Su C, Wang HH, Chen HS, Li TY, Chen BR, Chang CC, Li WR. Synthesis and characterization of carbene-pyridyl anchoring Ru(ii) dyes with various binding functionalities for photoelectrochemical cells. New J Chem 2018;42:15245-52.

[136] Ahmed U, Alizadeh M, Rahim NA, Shahabuddin S, Ahmed MS, Pandey AK. A comprehensive review on counter electrodes for dye sensitized solar cells: A special focus on Pt-TCO free counter electrodes. Sol Energy 2018;174:1097-125.

[137] Gong M, Kim JK, Zhao X, Li Y, Zhang J, Huang M, Wu Y. Visible-light-induced a-oxyamination of 1,3-dicarbonyls with TEMPO: Via a photo(electro)catalytic process applying a DSSC anode or in a DSSC system. Green Chem 2019;21:3615-20.

[138] Tangtrakarn A, Maiaugree W, Uppachai P, Ratchapolthavisin N, Moolsarn K, Swatsitang E, Amornkitbamrung V. High stability arc-evaporated carbon counter electrodes in a dye sensitized solar cell based on inorganic and organic redox mediators. Diamond Relat Mater 2019;97:107451.

[139] Adamovic N, Zimmermann A, Caviasca A, Harboe R, Ibanez F. Custom designed photovoltaic modules for PIPV and BIPV applications. J Renewable Sustainable Energy 2017;9:021202.

[140] Reich NH, van Sark WGJHM, Turkenburg WC. Charge yield potential of indoor-operated solar cells incorporated into product integrated photovoltaic (PIPV). Renewable Energy 2011;36:642-7.

[141] Dokouzis A, Bella F, Theodosiou K, Gerbaldi C, Leftheriotis G. Photoelectrochromic devices with cobalt redox electrolytes. Mater Today Energy 2020;15:100365.

[142] Huan TN, Dalla Corte DA, Lamaison S, Karapinar D, Lutz L, Menguy N, Foldyna M, Turren-Cruz SH, Hagfeldt A, Bella F, Fontecave M, Mougel V. Low-cost high-efficiency system for solar-driven conversion of CO_2 to hydrocarbons. Proc. Natl. Acad. Sci. U.S.A. 2019;116:9735-40.

[143] Pedico A, Lamberti A, Gigot A, Fontana M, Bella F, Rivolo P, Cocuzza M, Pirri CF. High-performing and stable wearable supercapacitor exploiting rGO aerogel decorated with copper and molybdenum sulfides on carbon fibers. ACS Appl. Energy Mater. 2018;1:4440-7.

[144] Rajan AK, Cindrella L. Photovoltaic properties of Cassia fistula flower extract based dye-sensitized solar cells. J Nanophotonics 2019;13:036007.

[145] Xie Y, Zhou H, Zhang S, Ge C, Cheng S. Influence of the auxiliary acceptor and p-bridge in triarylamine dyes on dye-sensitized solar cells. Photochem Photobiol Sci 2019;18:2042-51.

[146] Fagiolari L, Bella F. Carbon-based materials for stable, cheaper and large-scale processable perovskite solar cells. Energy Environ Sci 2019;12:3437-72.

[147] Bella F, Porcarelli L, Mantione D, Gerbaldi C, Barolo C, Grätzel M, Mecerreyes D. A water-based and metal-free dye solar cell exceeding 7% efficiency using a cationic poly(3,4-ethylenedioxythiophene) derivative. Chem Sci 2020;11:1485-93.

[148] Carella A, Centore R, Borbone F, Toscanesi M, Trifuoggi M, Bella F, Gerbaldi C, Galliano S, Schiavo E, Massaro A, Muñoz-García AB, Pavone M. Tuning optical and electronic properties in novel carbazole photosensitizers for p-type dye-sensitized solar cells. Electrochim Acta 2018;292:805-16.

[149] Xue Q, Xia R, Brabec CJ, Yip HL. Recent advances in semi-transparent polymer and perovskite solar cells for power generating window applications. Energy Environ Sci 2018;11:1688-709.

[150] PVeducation, https://www.pveducation.org/pvcdrom/solar-cell-operation/solar-cell-efficiency, accessed May 2020.

[151] Wan C, Jiao Y, Liang D, Wu Y, Li J. A high-performance, all-textile and spirally wound asymmetric supercapacitors based on core–sheath structured MnO_2 nanoribbons and cotton-derived carbon cloth. Electrochim Acta 2018;285:262-71.

[152] Al-Hada NM, Kamari HM, Abdullah CAC, Saion E, Shaari AH, Talib ZA, Matori KA. Down-top nanofabrication of binary $(CdO)_x(ZnO)_{1-x}$ nanoparticles and their antibacterial activity. Int J Nanomed 2017;12:8309-23.

[153] Anas S, Nair PV, Mahesh KV, Linsha V, Shuhailath A, Mohamed AP, Warrier KGK, Ananthakumar S. Engineered hetero structured arrays of ZnO NanoX (X = discs, rods and wires) and CdTe quantum dots for advanced electron transport applications. Mater Des 2018;141:267-75.

[154] Kathiravan D, Huang BR. Concurrent enhancement in the H_2 and UV sensing properties of ZnO nanostructures through discontinuous lattice coating of La^{3+}: Via partial p-n junction formation. J Mater Chem C 2018;6:2387-95.

[155] Liu N, Xue H, Ji Y, Wang J. ZnSe/ZnS core-shell quantum dots incorporated with Ag nanoparticles as luminescent down-shifting layers to enhance the efficiency of Si solar cells. J. Alloys Compd. 2018;747:696-702.

[156] Liu S, Qiao X, Wang Y, Xie H, Zhang N, Liu D. Magnetic and optical behaviors of SnO_{2-x} thin films with oxygen vacancies prepared by atomic layer deposition. Ceram Int 2019;45:4128-32.

[157] Pramanik A, Biswas S, Tiwary CS, Sarkar R, Kumbhakar P. Colloidal N-doped graphene quantum dots with tailored luminescent downshifting and detection of UVA radiation with enhanced responsivity. ACS Omega 2018;3:16260-70.

[158] Ghosh S, Mallik AK, Basu RN. Enhanced photocatalytic activity and photoresponse of poly(3,4-ethylenedioxythiophene) nanofibers decorated with gold nanoparticle under visible light. Sol Energy 2018;159:548-60.

[159] Khan A, Nair V, Colmenares JC, Gläser R. Lignin-based composite materials for photocatalysis and photovoltaics. Top. Curr. Chem. 2018;376:20.

[160] Jaramillo-Páez C, Sánchez-Cid P, Navío JA, Hidalgo MC. A comparative assessment of the UV-photocatalytic activities of ZnO synthesized by different routes. J Environ Chem Eng 2018;6:7161-71.

[161] Mandal AK, Diers JR, Niedzwiedzki DM, Hu G, Liu R, Alexy EJ, Lindsey JS, Bocian DF, Holten D. Tailoring panchromatic absorption and excited-state dynamics of tetrapyrrole-chromophore (bodipy, rylene) arrays - Interplay of orbital mixing and configuration interaction. J Am Chem Soc 2017;139:17547-64.

[162] Kumar S, Shandilya M, Thakur S, Thakur N. Structural, optical and photoluminescence properties of $K_{0.5}Na_{0.5}NbO_3$ ceramics synthesized by sol–gel reaction method. J Sol-Gel Sci Technol 2018;88:646-53.

[163] Sgibnev Y, Cattaruzza E, Dubrovin V, Vasilyev V, Nikonorov N. Photo-thermo-refractive glasses doped with silver molecular clusters as luminescence downshifting material for photovoltaic applications. Part Part Syst Char 2018;35:1800141.

[164] El-Bashir SM, Alwadai NM. Fullerene C_{60} doped polymeric nanocomposite coatings: moving solar spectra from ultraviolet to the deep red. J Mater Sci - Mater Electron 2018:29:19652-62.

[165] Valiev RR, Drozdova AK, Petunin PV, Postnikov PS, Trusova ME, Cherepanov VN, Sundholm D. The aromaticity of verdazyl radicals and their closed-shell charged species. New J Chem 2018;42:19987-94.

[166] Wei YX, Ma YB, Chen M, Liu WM, Li L, Yan Y. Electrochemical investigation of electrochromic device based on WO_3 and Ti doped V_2O_5 films by using electrolyte containing ferrocene. J Electroanal Chem 2017;807:45-51.

[167] Pan M, Ke Y, Ma L, Zhao S, Wu N, Xiao D. Single-layer electrochromic device based on hydroxyalkyl viologens with large contrast and high coloration efficiency. Electrochim Acta 2018;266:395-403.

[168] Pang Y, Tao Y, Zhang C, Cheng H. Fast switching soluble electrochromic polymers obtained from a 4,9-dihydro-s-indaceno[1,2-b:5,6-b']dithiophene-embedded system. Synth Met 2018;242:29-36.

[169] Kim SU, Lee SH, Sim J, Lee SD, Na JH. Topographic localization of liquid crystals based on gradual phase separation in a polymer network for electrically tunable smart window applications. J Inf Disp 2018;19:151-7.

[170] Xu F, Wu X, Zheng J, Xu C. A new strategy to fabricate multicolor electrochromic device with UV-detecting performance based on TiO_2 and PProDOT-Me_2. Org Electron 2019;65:8-14.

[171] Wu ZF, Tan B, Ma W, Xiong WW, Xie ZL, Huang XY. Mg^{2+} incorporated Co-based MOF precursors for hierarchical CNT-containing porous carbons with ORR activity. Dalton Trans 2018;47:2810-9.

[172] Soellner J, Strassner T. Diaryl-1,2,3-triazolylidene platinum(II) complexes. Chem Eur J 2018;24:5584-90.

[173] Gao X, Zhang T. An overview: Facet-dependent metal oxide semiconductor gas sensors. Sens Actuators, B 2018;277:604-33.

[174] Palma-Ramírez D, Domínguez-Crespo MA, Torres-Huerta AM, Escobar-Barrios VA, Dorantes-Rosales H, Willcock H. Dispersion of upconverting nanostructures of $CePO_4$ using rod and semi-spherical morphologies into transparent PMMA/PU IPNs by the sequential route. Polymer 2018;142:356-74.

[175] Zhang XP, Jiang WL, Cao SH, Sun HJ, You XQ, Cai SH, Wang JL, Zhao CS, Wang X, Chen Z, Sun SG. NMR spectroelectrochemistry in studies of hydroquinone oxidation by polyaniline thin films. Electrochim Acta 2018;273:300-6.

[176] Yu X, Zhang Y, Jin L, Chen J, Jiang Z, Zhang Y. High-performance piezo-damping materials based on CNTs/$BaTiO_3$/F-PAEK-b-PDMS under high temperature steam conditions. Appl Surf Sci 2018;452:429-36.

[177] Liu C, Zhang Z, Qu R. Hydrothermal synthesis of MoS_2/CC composite with enhanced photo-degradation activity and easy recycle property. J Mater Sci - Mater Electron 2018;29:18238-48.

[178] Matson SM, Litvinova EG, Khotimskiy VS. Membrane materials with semi-interpenetrating networks based on poly(4-methyl-2-pentyne) and polyethyleneimine. Pet Chem 2018;58:934-40.

[179] Zhang X, He J, Yue L, Bai Y, Liu H. Heat resistance of acrylic pressure-sensitive adhesives based on commercial curing agents and UV/heat curing systems. J Appl Polym Sci 2019;136:47310.

[180] Abdullah OG, Aziz SB, Saber DR. Characterization of pure and Pb^{2+} ion doped methylcellulose based biopolymer electrolyte films: Optical and electrical properties. Int J Electrochem Sci 2018;13:11931-52.

[181] Kim MK, Lee JS. Short-term plasticity and long-term potentiation in artificial biosynapses with diffusive dynamics. ACS Nano 2018;12:1680-7.

[182] Kim MK, Lee JS. Ultralow power consumption flexible biomemristors. ACS Appl Mater Interfaces 2018;10:10280-6.

[183] Chen S, Song Y, Xu F. Highly transparent and hazy cellulose nanopaper simultaneously with a self-cleaning superhydrophobic surface. ACS Sustainable Chem Eng 2018;6:5173-81.

[184] Wang S, Xu Z, Wang T, Xiao T, Hu XY, Shen YZ, Wang L. Warm/cool-tone switchable thermochromic material for smart windows by orthogonally integrating properties of pillar[6]arene and ferrocene. Nat Commun 2018;9:1737.

[185] Zhi H, Fei X, Tian J, Zhao L, Zhang H, Jing M, Xu L, Wang Y, Li Y. A novel high-strength photoluminescent hydrogel for tissue engineering. Biomater Sci 2018;6:2320-6.

[186] Qin X, Wang S, Luo L, He G, Sun H, Gong Y, Jiang B, Wei C. AIE-active polyanetholesulfonic acid sodium salts with room-temperature phosphorescence characteristics for Fe^{3+} detection. RSC Adv 2018;8:31231-6.

[187] Petunin PV, Martynko EA, Trusova ME, Kazantsev MS, Rybalova TV, Valiev RR, Uvarov MN, Mostovich EA, Postnikov PS. Verdazyl radical building blocks: Synthesis, structure, and Sonogashira cross-coupling reactions. Eur J Org Chem 2018;2018:4802-11.

[188] Smith S, Korvink JG, Mager D, Land K. The potential of paper-based diagnostics to meet the ASSURED criteria. RSC Adv 2018;8:34012-34.

[189] Musazade E, Voloshin R, Brady N, Mondal J, Atashova S, Zharmukhamedov SK, Huseynova I, Ramakrishna S, Najafpour MM, Shen JR, Bruce BD, Allakhverdiev SI. Biohybrid solar cells: Fundamentals, progress, and challenges. J Photochem Photobiol, C 2018;35:134-56.

[190] Sahu A, Tirosh S, Hiremath KR, Zaban A, Dixit A. A novel process for sensitization and infiltration of quantum dots in mesoporous metal oxide matrix for efficient solar photovoltaics response. Sol Energy 2018;169:488-97.

[191] Nandani, Supriyanto A, Ramelan AH, Nurosyid F. Effect of annealing temperature on optical properties of TiO_2 18 NR-T type thin film. J Phys Conf Ser 2018;1011:012016.

[192] Mei X, Wu B, Guo X, Liu X, Rong Z, Liu S, Chen Y, Qin D, Xu W, Hou L, Chen B. Efficient CdTe nanocrystal/TiO_2 hetero-junction solar cells with open circuit voltage breaking 0.8 V by incorporating a thin layer of CdS nanocrystal. Nanomaterials 2018;8:614.

[193] Zhang X, Rui Y, Yang J, Wang L, Wang Y, Xu J. Monodispersed SnO_2 microspheres aggregated by tunable building units as effective photoelectrodes in solar cells. Appl Surf Sci 2019;463:679-85.

[194] Fu X, Xu L, Li J, Sun X, Peng H. Flexible solar cells based on carbon nanomaterials. Carbon 2018;139:1063-73.

[195] Jiang CY, Liu HN, Zhang FB, Ji FY, Xu S, Wan Y. Application of photonic crystal in solar cells. Rengong Jingti Xuebao/Journal of Synthetic Crystals 2018;47:292-6.

[196] Sadasivuni KK, Deshmukh K, Ahipa TN, Muzaffar A, Ahamed MB, Pasha SKK, Al-Maadeed MAA. Flexible, biodegradable and recyclable solar cells: A review. J Mater Sci - Mater Electron 2019;30:951-74.

[197] Estrella LL, Kim DH. Theoretical design and characterization of NIR porphyrin-based sensitizers for applications in dye-sensitized solar cells. Sol Energy 2019;188:1031-40.

[198] Shi X, Liao X, Gao K, Zuo L, Chen J, Zhao J, Liu F, Chen Y, Jen AKY. An electron acceptor with broad visible–NIR absorption and unique solid state packing for as-cast high performance binary organic solar cells. Adv Funct Mater 2018;28:1802324.

[199] Tang J, Zhang Y, Zheng G, Gou J, Wu F. Improving the NIR light-harvesting of perovskite solar cell with upconversion fluorotellurite glass. J Am Ceram Soc 2018;101:1923-8.

[200] Boopathi KM, Hanmandlu C, Singh A, Chen YF, Lai CS, Chu CW. UV- and NIR-protective semitransparent smart windows based on metal halide solar cells. ACS Appl Energy Mater 2018;1:632-7.

[201] Li TY, Meyer T, Meerheim R, Höppner M, Körner C, Vandewal K, Zeika O, Leo K. Aza-BODIPY dyes with heterocyclic substituents and their derivatives bearing a cyanide co-ligand: NIR donor materials for vacuum-processed solar cells. J Mater Chem A 2017;5:10696-703.

[202] Lunt RR, Bulovic V. Transparent, near-infrared organic photovoltaic solar cells for window and energy-scavenging applications. Appl Phys Lett 2011;98:113305.

[203] MIT Energy Initiative, http://energy.mit.edu/news/transparent-solar-cells/, accessed May 2020.

[204] Chen CC, Dou L, Zhu R, Chung CH, Song TB, Zheng YB, Hawks S, Li G, Weiss PS, Yang Y. Visibly transparent polymer solar cells produced by solution processing. ACS Nano 2012;6:7185-90.

[205] Kamat PV. Quantum dot solar cells. Semiconductor nanocrystals as light harvesters. J Phys Chem C 2008;112:18737-53.

[206] Zhang X, Hägglund C, Johansson MB, Sveinbjörnsson K, Johansson EMJ. Fine tuned nanolayered metal/metal oxide electrode for semitransparent colloidal quantum dot solar cells. Adv Funct Mater 2016;26:1921-9.

[207] Kojima A, Teshima K, Shirai Y, Miyasaka T. Organometal halide perovskites as visible-light sensitizers for photovoltaic cells. J Am Chem Soc 2009;131:6050-1.

[208] Sun PP, Kripalani DR, Bai L, Zhou K. Prediction of the role of bismuth dopants in organic-inorganic lead halide perovskites on photoelectric properties and photovoltaic performance. J Phys Chem C 2019;123:12684-93.

[209] Yu D, Hu Y, Shi J, Tang H, Zhang W, Meng Q, Han H, Ning Z, Tian H. Stability improvement under high efficiency-next stage development of perovskite solar cells. Science China-Chemistry 2019;62:684-707.

[210] Liu Z, Li S, Wang X, Cui Y, Qin Y, Leng S, Xu YX, Yao K, Huang H. Interfacial engineering of front-contact with finely tuned polymer interlayers for high-performance large-area flexible perovskite solar cells. Nano Energy 2019;62:734-44.

[211] Zhang S, Wu S, Chen R, Chen W, Huang Y, Zhu H, Yang Z, Chen W. Controlling orientation diversity of mixed ion perovskites: Reduced crystal microstrain and improved structural stability. J Phys Chem Lett 2019;10:2898-903.

[212] Tu J, Liu C, Fan Y, Liu F, Chang K, Xu Z, Li Q, Chen Y, Li Z. Enhanced performance and stability of p-i-n perovskite solar cells by utilizing an AIE-active cathode interlayer. J Mater Chem A 2019;7:15662-72.

[213] Li X, Ding HH, Li GH, Wang Y, Fang ZM, Yang SF, Ju HX, Zhu JF. In situ investigations of interfacial degradation and ion migration at $CH_3NH_3PbI_3$ perovskite/Ag interface. Chin J Chem Phys 2019;32:299-305.

[214] Bai S, Da P, Li C, Wang Z, Yuan Z, Fu F, Kawecki M, Liu X, Sakai N, Wang JTW, Huettner S, Buecheler S, Fahlman M, Gao F, Snaith HJ. Planar perovskite solar cells with long-term stability using ionic liquid additives. Nature 2019;571:245-50.

[215] Gao L, Zhang F, Chen X, Xiao C, Larson BW, Dunfield SP, Berry JJ, Zhu K. Enhanced charge transport by incorporating formamidinium and cesium cations into two-dimensional perovskite solar cells. Angew Chem Int Ed 2019;58:11737-41.

[216] Wang K, Subhani WS, Wang Y, Zuo X, Wang H, Duan L, Liu SF. Metal cations in efficient perovskite solar cells: Progress and perspective. Adv Mater 2019;31:1902037.

[217] Shini F, Thambidurai M, Harikesh PC, Mathews N, Huang Y, Dang C. Heterogeneous electron transporting layer for reproducible, efficient and stable planar perovskite solar cells. J Power Sources 2019;437:226907.

[218] Guo P, Yang X, Ye Q, Zhang J, Wang H, Yu H, Zhao W, Liu C, Yang H, Wang H. Laser-generated nanocrystals in perovskite: Universal embedding of ligand-free and sub-10 nm nanocrystals in solution-processed metal halide perovskite films for effectively modulated optoelectronic performance. Adv Energy Mater 2019;9:1901341.

[219] Wusimanjiang Y, Yadav J, Arau V, Steen AE, Hammer NI, Pan S. Blue electrogenerated chemiluminescence from halide perovskite nanocrystals. J Anal Test 2019;3:125-33.

[220] Subair R, Di Girolamo D, Bodik M, Nadazdy V, Li B, Nadazdy P, Markovic Z, Benkovicova M, Chlpik J, Kotlar M, Halahovets Y, Siffalovic P, Jergel M, Tian J, Brunetti F, Majkova E. Effect of the doping of $PC_{61}BM$ electron transport layer with carbon nanodots on the performance of inverted planar $MAPbI_3$ perovskite solar cells. Sol Energy 2019;189:426-34.

[221] Pang Z, Sun Y, Gao Y, Zhang X, Sun Y, Yang J, Wang F, Yang L. Unravelling the mechanism of interface passivation engineering for achieving high-efficient ZnO-based planar perovskite solar cells. J Power Sources 2019;438:226957.

[222] Bella F, Renzi P, Cavallo C, Gerbaldi C. Caesium for perovskite solar cells: An overview. Chem Eur J 2018;24:12183-205.

[223] Zhou L, Katan C, Nie W, Tsai H, Pedesseau L, Crochet JJ, Even J, Mohite AD, Tretiak S, Neukirch AJ. Cation alloying delocalizes polarons in lead halide perovskites. J Phys Chem Lett 2019;10:3516-24.

[224] Ye QQ, Wang ZK, Femi I, Wang KL, Zhang Y, Ma XJ, Zhuo MP, Liao LS. A $SrGeO_3$ inorganic electron-transporting layer for high-performance perovskite solar cells. J Mater Chem A 2019;7:14559-64.

[225] Tavakoli MM, Dastjerdi HT, Prochowicz D, Yadav P, Tavakoli R, Saliba M, Fan Z. Highly efficient and stable inverted perovskite solar cells using down-shifting quantum dots as a light management layer and moisture-assisted film growth. J Mater Chem A 2019;7:14753-60.

[226] Tress W, Domanski K, Carlsen B, Agarwalla A, Alharbi EA, Graetzel M, Hagfeldt A. Performance of perovskite solar cells under simulated temperature-illumination real-world operating conditions. Nat Energy 2019;4:568-74.

[227] Pandey M, Kapil G, Sakamoto K, Hirotani D, Kamrudin MA, Wang Z, Hamada K, Nomura D, Kang HG, Nagayoshi H, Nakamura M, Hayashi M, Nomura T, Hayase S. Efficient, hysteresis free, inverted planar flexible perovskite solar cells: Via perovskite engineering and stability in cylindrical encapsulation. Sustainable Energy Fuels 2019;3:1739-48.

[228] Best Research-Cell Efficiency Chart by NREL, https://www.nrel.gov/pv/cell-efficiency.html, accessed May 2020.

[229] Roldán-Carmona C, Malinkiewicz O, Betancur R, Longo G, Momblona C, Jaramillo F, Camacho L, Bolink HJ. High efficiency single-junction semitransparent perovskite solar cells. Energy Environ Sci 2014;7:2968-73.

[230] Bailie CD, Christoforo MG, Mailoa JP, Bowring AR, Unger EL, Nguyen WH, Burschka J, Pellet N, Lee JZ, Grätzel M, Noufi R, Buonassisi T, Salleo A, McGehee MD. Semi-transparent perovskite solar cells for tandems with silicon and CIGS. Energy Environ Sci 2015;8:956-63.

[231] Teo BH, Khanna A, Shanmugam V, Aguilar MLO, Delos Santos ME, Chua DJW, Chang WC, Mueller T. Development of nanoparticle copper screen printing pastes for silicon heterojunction solar cells. Sol Energy 2019;189:179-85.

[232] Rong Y, Ming Y, Ji W, Li D, Mei A, Hu Y, Han H. Toward industrial-scale production of perovskite solar cells: screen printing, slot-die coating, and emerging techniques. J Phys Chem Lett 2018;9:2707-13.

[233] Jia HL, Chen YC, Ji L, Lin LX, Guan MY, Yang Y. Cosensitization of porphyrin dyes with new X type organic dyes for efficient dye-sensitized solar cells. Dyes Pigm 2019;163:589-93.

[234] Bakker TMA, Mathew S, Reek JNH. Lindqvist polyoxometalates as electrolytes in p-type dye sensitized solar cells. Sustainable Energy Fuels 2019;3:96-100.

[235] Farhana NK, Ramesh S, Ramesh K. Efficiency enhancement of dye-sensitized solar cell based gel polymer electrolytes using poly(vinyl butyral-co-vinyl alcohol-co-vinyl acetate)/tetrapropylammonium iodide. Mater Sci Semicond Process 2019;91:414-21.

[236] Lyu L, Tang P, Tong G, Han L. Molecular engineering and synthesis of symmetric metal-free organic sensitizers with A-p-D-p-A architecture for DSSC applications: the effect of bridge unit. J Iran Chem Soc 2019;16:2441-50.

[237] Kokal RK, Bhattacharya S, Cardoso LS, Miranda PB, Soma VR, Chetti P, Melepurath D, Raavi SSK. Low cost 'green' dye sensitized solar cells based on New Fuchsin dye with aqueous electrolyte and platinum-free counter electrodes. Sol Energy 2019;188:913-23.

[238] Renaud A, Nguyen TKN, Grasset F, Raissi M, Guillon V, Delabrouille F, Dumait N, Jouan PY, Cario L, Jobic S, Pellegrin Y, Odobel F, Cordier S, Uchikoshi T. Preparation by electrophoretic deposition of molybdenum iodide cluster-based functional nanostructured photoelectrodes for solar cells. Electrochim Acta 2019;317:737-45.

[239] Peiris DSU, Ekanayake P, Petra MI. Stacked rGO–TiO_2 photoanode via electrophoretic deposition for highly efficient dye-sensitized solar cells. Org Electron 2018;59:399-405.

[240] Adnan M, Lee JK. All sequential dip-coating processed perovskite layers from an aqueous lead precursor for high efficiency perovskite solar cells. Sci Rep 2018;8:2168.

[241] Pu D, Zhou W, Li Y, Chen J, Chen J, Zhang H, Mi B, Wang L, Ma Y. Order-enhanced silver nanowire networks fabricated by two-step dip-coating as polymer solar cell electrodes. RSC Adv 2015;5:100725-9.

[242] Zeng C, Liang Y, Zeng L, Zhang L, Zhou J, Huang P, Hong R. Effect of S/(S+Se) ratio during the annealing process on the performance of $Cu_2ZnSn(S,Se)_4$ solar cells prepared by sputtering from a quaternary target. Sol Energy Mater Sol Cells 2019;203:110167.

[243] Noh YJ, Kim JG, Kim SS, Kim HK, Na SI. Efficient semi-transparent perovskite solar cells with a novel indium zinc tin oxide top electrode grown by linear facing target sputtering. J Power Sources 2019;437:226894.

[244] Poulose AC, Veeranarayanan S, Varghese SH, Yoshida Y, Maekawa T, Sakthi Kumar D. Functionalized electrophoretic deposition of CdSe quantum dots onto TiO_2 electrode for photovoltaic application. Chem Phys Lett 2012;539-540:197-203.

[245] Ossila Ltd., https://www.ossila.com/pages/solution-processing-techniques-comparison, accessed May 2020.

[246] Thin Film Consulting, http://www.thfc.de/fundamentals-of-sputtering, accessed May 2020.

[247] Bushra N, Hartmann T. A review of state-of-the-art reflective two-stage solar concentrators: Technology categorization and research trends. Renewable Sustainable Energy Rev 2019;114:109307.

[248] Mazzaro R, Vomiero A. The renaissance of luminescent solar concentrators: The role of inorganic nanomaterials. Adv Energy Mater 2018;8:1801903.

[249] Yang C, Lunt RR. Limits of visibly transparent luminescent solar concentrators. Adv Opt Mater 2017;5:1600851.

[250] Chen RT, Chau JLH, Hwang GL. Design and fabrication of diffusive solar cell window. Renewable Energy 2012;40:24-8.

[251] Zhao Y, Meek GA, Levine BG, Lunt RR. Near-infrared harvesting transparent luminescent solar concentrators. Adv Opt Mater 2014;2:606-11.

[252] Lavagna L, Nisticò R, Sarasso M, Pavese M. An analytical mini-review on the compression strength of rubberized concrete as a function of the amount of recycled tires crumb rubber. Materials 2020;13:1234.

[253] Alberghini M, Morciano M, Bergamasco L, Fasano M, Lavagna L, Humbert G, Sani E, Pavese M, Chiavazzo E, Asinari P. Coffee-based colloids for direct solar absorption. Sci Rep 2019;9:4701.

[254] Lavagna L, Nisticò R, Chiappone A, Pavese M. Facile photo-induced growth of polymeric nanostructures onto cellulose: The poly(ethylene glycol) methacrylate (PEGMA)@cellulose case study. Mater Lett 2018;227:202-4.

[255] Lavagna L, Nisticò R, Musso S, Pavese M. Hydrophobic cellulose ester as a sustainable material for simple and efficient water purification processes from fatty oils contamination. Wood Sci Technol 2019;53:249-61.

[256] Lavagna L, Musso S, Ferro G, Pavese M. Cement-based composites containing functionalized carbon fibers. Cem Concr Compos 2018;88:165-71.

[257] Lavagna L, Massella D, Pantano MF, Bosia F, Pugno NM, Pavese M. Grafting carbon nanotubes onto carbon fibres doubles their effective strength and the toughness of the composite. Compos. Sci. Technol. 2018;166:140-9.

[258] Ito S, Chen P, Comte P, Nazeeruddin MK, Liska P, Péchy P, Grätzel M. Fabrication of screen-printing pastes from TiO_2 powders for dye-sensitised solar cells. Prog Photovoltaics Res Appl 2007;15:603-12.

[259] Chen KS, Salinas JF, Yip HL, Huo L, Hou J, Jen AKY. Semi-transparent polymer solar cells with 6% PCE, 25% average visible transmittance and a color rendering index close to 100 for power generating window applications. Energy Environ Sci 2012;5:9551-7.

[260] Zhang J, Li S, Yang P, Que W, Liu W. Deposition of transparent TiO_2 nanotubes-films via electrophoretic technique for photovoltaic applications. Sci China Mater 2015;58:785-90.

[261] Bahramian A, Vashaee D. In-situ fabricated transparent conducting nanofiber-shape polyaniline/coral-like TiO_2 thin film: Application in bifacial dye-sensitized solar cells. Sol Energy Mater Sol Cells 2015;143:284-95.

[262] Zhang X, Eperon GE, Liu J, Johansson EMJ. Semitransparent quantum dot solar cell. Nano Energy 2016;22:70-8.

[263] D.M. 26/6/2015 - appendix B. “Applicazione delle metodologie di calcolo delle prestazioni energetiche e definizione delle prescrizioni e dei requisiti minimi degli edifici”.

[264] UNI/TS 11300-1:2014. “Energy performance of buildings-Part 1: Evaluation of energy need for space heating and cooling”.

[265] Sygkridoua S, Rapsomanikisa A, Stathatos E. Transparent solar cells in large scale for energy harvesting in buildings. ICCMSE 2014.

[266] Photovoltaic Geographical Information System, https://re.jrc.ec.europa.eu/pvg_tools/en/tools.html, accessed May 2020.

[267] UNI EN 12464-1:2004. “Light and lighting - lighting of work places - part 1: indoor work places”.

[268] UNI EN ISO 13790:2008. “Energy performance of buildings - Calculation of energy use for space heating and cooling”.

[269] Sygkridou D, Rapsomanikis A, Stathatos E. Transparent solar cells in large scale for energy harvesting in buildings. AIP Conf Proc 2014;1618:366-9.

[270] Glass to Power SpA, www.glasstopower.com, accessed May 2020.

[271] PV Magazine, https://www.pv-magazine.com/2018/07/23/italy-glass-to-power-crowdfunds-e2-25-million-plans-solar-window-fab/, accessed May 2020.

[272] Vega-Garita V, Ramirez-Elizondo L, Narayan N, Bauer P. Integrating a photovoltaic storage system in one device: A critical review. Prog Photovoltaics Res Appl 2019;27:346-70.

[273] Di Carlo Rasi D, Janssen RAJ. Advances in solution-processed multijunction organic solar cells. Adv Mater 2019;31:1806499.

[274] Kang L, Zhang Z, Shi J, Yan R, Zhang J. Surface morphology control of Cu_2ZnSnS_4 by addition of cellulose in solution process for high performance superstrate solar cell. Mater Res Bull 2019;113:31-7.

[275] Dai D, Tu X, Li X, Lv T, Han F. Tuning solar absorption spectra via carbon quantum dots/VAE composite layer and efficiency enhancement for crystalline Si solar module. Prog Photovoltaics Res Appl 2019;27:283-9.

[276] Spies JA, Perets EA, Fisher KJ, Rudshteyn B, Batista VS, Brudvig GW, Schmuttenmaer CA. Collaboration between experiment and theory in solar fuels research. Chem Soc Rev 2019;48:1865-73.

[277] Kolay A, Das A, Ghosal P, Deepa M. New photoelectrochromic device with chromatic silica/tungsten oxide/copper hybrid film and photovoltaic polymer/quantum dot sensitized anode. ACS Appl Energy Mater 2018;1:4084-95.

[278] Zhao D, Lu Q, Su R, Li Y, Zhao M. Light harvesting and optical-electronic properties of two quercitin and rutin natural dyes. Appl Sci 2019;9:567.

[279] Saadiah MA, Samsudin AS. Study on ionic conduction of solid bio-polymer hybrid electrolytes based carboxymethyl cellulose (CMC)/polyvinyl alcohol (PVA) doped NH_4NO_3. AIC Conf Proc 2018;2030:020223.

[280] Shivanna S, Subramani NK, Swamy K, Nagaraj SK, Muthuraj JRB, Siddaramaiah H. Orange-red fluorescent polymer nanocomposite films with large stokes shift: An opto-electronic exercise. J Lumin 2019;208:488-94.

[281] Biswas Y, Banerjee P, Mandal TK. From polymerizable ionic liquids to poly(ionic liquid)s: Structure-dependent thermal, crystalline, conductivity, and solution thermoresponsive behaviors. Macromolecules 2019;52:945-58.

[282] Scarfato P, Schiavone N, Rossi G, Incarnato L. An easy route to wettability changes of polyethylene terephthalate-silicon oxide substrate films for high barrier applications, surface-modified with a self-assembled monolayer of fluoroalkylsilanes. Polymers 2019;11:257.

[283] Shivanna S, Subramani NK, Nagaraj SK, Mutturaj JRB, Basavaraj S. Patina-green coloured light emitting polycarbonate films: A synergistic extraction of improved UV endurance and considerate spectral down-conversion. J Lumin 2019;210:276-84.

[284] Rose MA, Bowen JJ, Morin SA. Emergent soft lithographic tools for the fabrication of functional polymeric microstructures. ChemPhysChem 2019;20:909-25.

[285] Wu W. Stretchable electronics: Functional materials, fabrication strategies and applications. Sci. Technol. Adv. Mater. 2019;20:187-224.

[286] Olmedo-Martínez JL, Meabe L, Basterretxea A, Mecerreyes D, Müller AJ. Effect of chemical structure and salt concentration on the crystallization and ionic conductivity of aliphatic polyethers. Polymers 2019;11:452.

[287] Wadatkar NS, Waghuley SA. Exploring the electrical and complex optical properties of as-synthesized thiophene-indole conducting copolymers. Heliyon 2019;5:e01534.

[288] Lestari WW, Shahab S, Novita TH, Tedra RA, Purnawan C, Arrozi USF, Ni'Maturrohmah D. Electrosynthesis of coordination polymers containing magnesium(II) and benzene 1,3,5-tricarboxylate: The influence of solvents and electrolytes toward the dimensionality. IOP Conf Ser: Mater Sci Eng 2019;509:012149.

[289] Xie XY, Wu F, Liu X, Tao WQ, Jiang Y, Liu XQ, Sun LB. Photopolymerization of metal-organic polyhedra: An efficient approach to improve the hydrostability, dispersity, and processability. Chem Commun 2019;55:6177-80.

[290] Galhoum AA, Elshehy EA, Tolan DA, El-Nahas AM, Taketsugu T, Nishikiori K, Akashi T, Morshedy AS, Guibal E. Synthesis of polyaminophosphonic acid-functionalized poly(glycidyl methacrylate) for the efficient sorption of La(III) and Y(III). Chem Eng J 2019;375:121932.

[291] Zhu T, Mao J, Cheng Y, Liu H, Lv L, Ge M, Li S, Huang J, Chen Z, Li H, Yang L, Lai Y. Recent progress of polysaccharide-based hydrogel interfaces for wound healing and tissue engineering. Adv Mater Interfaces 2019;6:1900761.

[292] Chen Z, Lau KKS. Suppressing crystallinity by nanoconfining polymers using initiated chemical vapor deposition. Macromolecules 2019;52:5183-91.

[293] Lin CL, Chen CY, Yu HF, Ho KC. Comparisons of the electrochromic properties of poly(hydroxymethyl 3,4-ethylenedioxythiophene) and poly(3,4-ethylenedioxythiophene) thin films and the photoelectrochromic devices using these thin films. Sol Energy Mater Sol Cells 2019;202:110132.

[294] Huang J, Chen H, Hao B, Dai W, Chen S. Copolymerization strategy to prepare polymethyl methacrylate-based copolymer with broad-band ultraviolet shielding and luminescent down-shifting properties. J Mater Sci 2019;54:14624-33.

[295] Dai X, Yu L, Zhang Y, Zhang L, Tan J. Polymerization-induced self-assembly via RAFT-mediated emulsion polymerization of methacrylic monomers. Macromolecules 2019;52:;7468-76.

[296] Zhao H, Zhang W, Wu Y, Yin X, Du C, Zhao W, Zhao L, Liu C. Polyether-based polyurethane solid electrolyte flexible encapsulation material based on electrostatic bonding. Gongneng Cailiao/Journal of Functional Materials 2019;50:07040-5.

[297] Yadav K, Kumar A, Sastry OS, Wandhare R. An assessment for the selection of weather profiles for performance testing of SPV pumps in Indian climate. Sol Energy 2019;179:11-23.

[298] Chen Y, Zhu J, Ma H, Chen L, Li R, Jin P. VO_2/nickel-bromine-ionic liquid composite film for thermochromic application. Sol Energy Mater Sol Cells 2019;196:124-30.

[299] Tu N, Van Bui H, Trung DQ, Duong AT, Thuy DM, Nguyen DH, Nguyen KT, Huy PT. Surface oxygen vacancies of ZnO: A facile fabrication method and their contribution to the photoluminescence. J Alloys Compd 2019;791:722-9.

[300] Bujewska P, Gorska B, Fic K. Redox activity of selenocyanate anion in electrochemical capacitor application. Synth Met 2019;253:62-72.

[301] Li S, Zhong L, Huang S, Wang D, Zhang F, Zhang G. A reactive fluorine-free, efficient superhydrophobic and flame-retardant finishing agent for cotton fabrics. Cellulose 2019:26:6333-47.

[302] Razmara Z, Abdelbaky MSM, García-Granda S. Synthesis and molecular structure of a new metal-organic complex based on Zn(II) and quinoline, a precursor for fabrication of ZnO nanoparticles applicable in the photocatalytic reactions. J. Mol. Struct. 2019;1197:217-26.

[303] Komal B, Yadav M, Kumar M, Tiwari T, Srivastava N. Modifying potato starch by glutaraldehyde and $MgCl_2$ for developing an economical and environment-friendly electrolyte system. E-Polymers 2019;19:453-61.

[304] Fu F, Zhang Y, Zhang Z, Zhang X, Chen Y, Zhang Y. The preparation and performance of Au loads TiO_2 nanomaterials. Mater. Res. Express 2019;6:095041.

[305] Erden S, Savaci U, Ozel E, Turan S, Suvaci E. Investigation of the chemical stability of Zn_2SnO_4 in aqueous media by using ICP-OES and TEM analyses. Mater. Chem. Phys. 2020;239:122066.

[306] Wang X, Li Y, Song P, Ma F, Yang Y. Second-order nonlinear optical switch manipulation of photosensitive layer by an external electric field coupled with graphene quantum dots. J Phys Chem A 2019;123:7401-7.

[307] Shen H, Gu Z, Zheng G. Pushing the activity of CO_2 electroreduction by system engineering. Sci Bull 2019;64:1805-16.

[308] Ji SH, Cho YS, Yun JS. Wearable core-shell piezoelectric nanofiber yarns for body movement energy harvesting. Nanomaterials 2019;9:555.

[309] Wu S, Yang X, Zhao Y. Ru(II) bipyridyl complex and TiO_2 nanocomposite based biomolecule-free photoelectrochemical sensor for highly selective determination of ultra-trace Hg^{2+} in aqueous systems. Chem Res Chin Univ 2019;35:370-6.

[310] Kunene T, Xiong L, Rosenthal J. Solar-powered synthesis of hydrocarbons from carbon dioxide and water. Proc. Natl. Acad. Sci. U.S.A. 2019;116:9693-5.

[311] Kim J, Kwon EE. Photoconversion of carbon dioxide into fuels using semiconductors. J CO_2 Util 2019;33:72-82.

[312] Haldar R, Batra K, Marschner SM, Kuc AB, Zahn S, Fischer RA, Bräse S, Heine T, Wöll C. Bridging the green gap: Metal–organic framework heteromultilayers assembled from porphyrinic linkers identified by using computational screening. Chem Eur J 2019;25:7847-51

[313] Chew YH, Tang JY, Tan LJ, Choi BWJ, Tan LL, Chai SP. Engineering surface oxygen defects on tungsten oxide to boost photocatalytic oxygen evolution from water splitting. Chem Commun 2019;55:6265-8.

[314] Kim HN, Yang S. Responsive smart windows from nanoparticle–polymer composites. Adv Funct Mater 2020;30:1902597.

[315] Karmakar S, Kumbhakar P, Maity K, Mandal D, Kumbhakar P. Development of flexible self-charging triboelectric power cell on paper for temperature and weight sensing. Nano Energy 2019;63:103831.

[316] Kim Y, Lee D, Kim SY, Kang E, Kim CK. Nanocomposite synthesis of nanodiamond and molybdenum disulfide. Nanomaterials 2019;9:927.

[317] Wakerley D, Lamaison S, Ozanam F, Menguy N, Mercier D, Marcus P, Fontecave M, Mougel V. Bio-inspired hydrophobicity promotes CO_2 reduction on a Cu surface. Nat Mater 2019;18:1222-7.

[318] Güzel R, Ocak YS, Karuk SN, Ersöz A, Say R. Light harvesting and photo-induced electrochemical devices based on bionanocage proteins. J Power Sources 2019;440:227119.

[319] Chiu KL, Shang S, Wang Y, Jiang S. A novel template-free wet chemical synthesis method for economical production of zinc oxide microrods under atmospheric pressure. Ceram Int 2019;46:2002-9.

[320] Tang D, Zhao R, Shen C, Han Y, Wu X, Wu H, Diao G, Chen M. High electrocatalytic performance of bimetallic sulfides dodecahedral nanocages ($Co_xM_{1-x})_9S_8$/M/N–C (M=Ni, Cu) for triiodide reduction reaction and oxygen evolution reaction. Electrochim Acta 2019;324:134888.

[321] Kuang ZY, Deng Y, Hu J, Tao L, Wang P, Chen J, Xie HL. Responsive smart windows enabled by the azobenzene copolymer brush with photothermal effect. ACS Appl Mater Interfaces 2019;11:37026-34.

[322] Torres FG, Ccorahua R, Arroyo J, Troncoso OP. Enhanced conductivity of bacterial cellulose films reinforced with NH_4I-doped graphene oxide. Pol-Plast Technol Mater 2019;58:1585-95.

[323] Naceur Abouloula C, Rizwan M, Selvanathan V, Hassan A, Yahya R, Oueriagli A. Oil palm waste based phthaloyl cellulose: a product of photosynthesis as an electrolyte of photovoltaics. Cellulose 2019;26:1605-17.

[324] Soganci T, Ak M. An eco-friendly method to enhance optical and electrical properties of conducting polymers by means of carboxymethyl cellulose. Cellulose 2019;26:2541-55.

[325] Brunetti F, Operamolla A, Castro-Hermosa S, Lucarelli G, Manca V, Farinola GM, Brown TM. Printed solar cells and energy storage devices on paper substrates. Adv Funct Mater 2019;29: 1806798.

[326] Wang G, Chen Y, Xu G, Pei Y. Effective removing of methylene blue from aqueous solution by tannins immobilized on cellulose microfibers. Int J Biol Macromol 2019;129:198-206.

[327] Lämmermann N, Schmid-Michels F, Weißmann A, Wobbe L, Hütten A, Kruse O. Extremely robust photocurrent generation of titanium dioxide photoanodes bio-sensitized with recombinant microalgal light-harvesting proteins. Sci Rep 2019;9:2109.

[328] Silakul P, Magaraphan R. Polymer electrolyte from natural rubber-polyacrylic acid and polypyrrole and its application. Macromol Res 2019;27:126-39.

[329] Nunes SC, Saraiva SM, Pereira RFP, Silva MM, Carlos LD, Almeida P, Gonçalves MC, Ferreira RAS, De Zea Bermudez V. Luminescent κ-carrageenan-based electrolytes containing neodymium triflate. Molecules 2019;24:1020.

[330] Lee BM, Eom JJ, Baek GY, Hong SK, Jeun JP, Choi JH, Yun JM. Cellulose non-woven fabric-derived porous carbon films as binder-free electrodes for supercapacitors. Cellulose 2019;26:4529-40.

[331] Ge J, Zhang S, Liu Z, Xie Z, Pan S. Flexible artificial nociceptor using a biopolymer-based forming-free memristor. Nanoscale 2019;11:6591-601.

[332] Jin Z, Che Y. Progress in cellulose nanocrystals and its application in hydrogels. Gaofenzi Cailiao Kexue Yu Gongcheng/Polymeric Materials Science and Engineering 2019;35:183-90.

[333] Hwang H, Jeong U. Microparticle-based soft electronic devices: Toward one-particle/one-pixel. Adv Funct Mater 2020;30:1901810.

[334] Rajkumar R, Shivakumar MS, Senthil Nathan S, Selvam K. Preparation and characterization of chitosan nanocomposites material using silver nanoparticle synthesized Carmona retusa (Vahl) Masam leaf extract for antioxidant, anti-cancerous and insecticidal application. J Cluster Sci 2019;30:1145-55.

[335] Feng X, Wu Z, Xie Y, Wang S. Reinforcing 3D print methacrylate resin/cellulose nanocrystal composites: Effect of cellulose nanocrystal modification. BioResources 2019;14:3701-16.

[336] Massella D, Giraud S, Guan J, Ferri A, Salaün F. Textiles for health: A review of textile fabrics treated with chitosan microcapsules. Environ Chem Lett 2019;17:1787-1800.

[337] Barra T, Arrue L, Urzúa E, Ratjen L. Synthesis of photocaged diamines and their application in photoinduced self-assembly. J Phys Org Chem 2019;32:e3935.

[338] Barcaro G, Monti S, Sementa L, Carravetta V. Modeling nucleation and growth of ZnO nanoparticles in a low temperature plasma by reactive dynamics. J Chem Theory Comput 2019;15:2010-21.

[339] Banasz R, Walesa-Chorab M. Polymeric complexes of transition metal ions as electrochromic materials: Synthesis and properties. Coord Chem Rev 2019;389:1-18.

[340] Troian-Gautier L, Turlington MD, Wehlin SAM, Maurer AB, Brady MD, Swords WB, Meyer GJ. Halide photoredox chemistry. Chem Rev 2019;119:4628-83.

[341] Savastano M, Martínez-Camarena Á, Bazzicalupi C, Delgado-Pinar E, Llinares JM, Mariani P, Verdejo B, García-España E, Bianchi A. Stabilization of supramolecular networks of polyiodides with protonated small tetra-azacyclophanes. Inorganics 2019;7:48.

[342] Yang X, Wang Y, Qi W, Yang B, Liu X, Zhang L, Liu J, Su R, He Z. Construction of supramolecular nanostructures with high catalytic activity by photoinduced hierarchical co-assembly. Chem Eur J 2019;25:7896-902.

[343] Lei J, Akitoshi T, Katou S, Murakami Y, Yin J, Jiang X. 9,10-dithio/oxo-anthracene as a novel photosensitizer for photoinitiator systems in photoresists. Macromol Chem Phys 2019;220:1900152.

[344] Draganov AB, Yang X, Anifowose A, De La Cruz LKC, Dai C, Ni N, Chen W, De Los Santos Z, Gu L, Zhou M, Wang B. Upregulation of p53 through induction of MDM2 degradation: Anthraquinone analogs. Bioorg. Med. Chem. 2019;27:3860-5.